ADVANCED ENERGY MATERIALS
www.advenergymat.de

Design Strategies, Practical Considerations, and New Solution Processes of Sulfide Solid Electrolytes for All-Solid-State Batteries

Kern Ho Park, Qiang Bai, Dong Hyeon Kim, Dae Yang Oh, Yizhou Zhu, Yifei Mo, and Yoon Seok Jung**

Owing to the ever-increasing safety concerns about conventional lithium-ion batteries, whose applications have expanded to include electric vehicles and grid-scale energy storage, batteries with solidified electrolytes that utilize nonflammable inorganic materials are attracting considerable attention. In particular, owing to their superionic conductivities (as high as ≈10^{-2} S cm^{-1}) and deformability, sulfide materials as the solid electrolytes (SEs) are considered the enabling material for high-energy bulk-type all-solid-state batteries. Herein the authors provide a brief review on recent progress in sulfide Li- and Na-ion SEs for all-solid-state batteries. After the basic principles in designing SEs are considered, the experimental exploration of multicomponent systems and ab initio calculations that accelerate the search for stronger candidates are discussed. Next, other issues and challenges that are critical for practical applications, such as instability in air, electrochemical stability, and compatibility with active materials, are discussed. Then, an emerging progress in liquid-phase synthesis and solution process of SEs and its relevant prospects in ensuring intimate ionic contacts and fabricating sheet-type electrodes is highlighted. Finally, an outlook on the future research directions for all-solid-state batteries employing sulfide superionic conductors is provided.

1. Introduction

Ubiquitous mobile electronic devices such as smartphones were indebted to the development of lithium-ion batteries (LIBs) having high energy and power density and good rechargeability. Since the first demonstration of prototype Li batteries (TiS_2/Li) in 1976,[1] the development of LIBs to date has been strongly affected by safety issues. One of the major technical breakthroughs for the commercialization of LIBs was the replacement of Li metal with carbonaceous materials as the anode.[2–4] It is well known that the use of Li metal was challenged by serious safety concerns associated with internal short circuit by the dendritic growth of Li metal.[5–7] The ever-rising requirements for higher energy density of LIBs have raised more serious safety concerns. Raising the upper cutoff voltages leads to poorer stability at electrode–electrolyte interfaces.[8,9] Ultrathinning the polymeric separators to less than 10 µm, despite the reinforcements using ceramic materials,[10–12] result in more vulnerability toward internal short circuits. These may also be related to degassing, fire, and explosion accidents of LIBs in recent years. Furthermore, large-scale applications of LIBs, such as battery-driven electric vehicles and grid-scale energy storages, face unprecedented challenges in terms of safety requirements.[13–15] In this regard, solidification of conventional flammable organic liquid electrolytes with inorganic materials, such as superionic conductor solid electrolytes (SEs), is an ideal solution.[16–25] Another strong motivation in the development of SEs is to unleash the harness of limited energy density for conventional LIBs by using SEs to stabilize and enable alternative high-capacity electrode materials, such as Li metal anode and sulfur cathode.[15,23] Additionally, the design of all-solid-state Li or Li-ion batteries (ALSBs) by stacking bipolar electrodes allows the minimization of inactive encasing materials, thereby increasing cell-level energy density.[22,26]

The first superionic conductors PbF_2 and Ag_2S were discovered by Michael Faraday in 1838.[27] Since then, several notable progresses in the field of solid-state superionic conductors and their newly enabled electrochemical devices had occurred;[27] the development of oxygen-ion conductors (Y-doped ZrO_2) applied to solid oxide fuel cells, the discoveries of Ag^+ superionic conductors (e.g., $RbAg_4I_5$), and the development of Na-ion conducting sodium beta alumina (β''-Al_2O_3). Currently, it is a promising opportunity for Li-ion SEs to revolutionize LIB technologies

Dr. K. H. Park, D. H. Kim, D. Y. Oh, Prof. Y. S. Jung
Department of Energy Engineering
Hanyang University
Seoul 04763, South Korea
E-mail: yoonsjung@hanyang.ac.kr
Q. Bai, Y. Zhu, Prof. Y. Mo
Department of Materials Science and Engineering
University of Maryland
College Park, MD 20742, USA
E-mail: yfmo@umd.edu
D. H. Kim, D. Y. Oh
School of Energy and Chemical Engineering
UNIST (Ulsan National Institute of Science and Technology)
Ulsan 44919, South Korea
The ORCID identification number(s) for the author(s) of this article can be found under https://doi.org/10.1002/aenm.201800035.

DOI: 10.1002/aenm.201800035

for practical applications. Recently, the developments of several state-of-the-art sulfide superionic conductor materials, such as $Li_{10}GeP_2S_{12}$ (LGPS) and $Li_{9.54}Si_{1.74}P_{1.44}S_{11.7}Cl_{0.3}$ (LSiPSCl), showing extremely high ionic conductivities reaching the order of 10^{-2} S cm^{-1},[16,22] have enabled ASLBs with outstanding electrochemical performance.

Figure 1a illustrates the bulk-type ASLBs, which are comprised of composite-structured electrodes, as commonly in the conventional LIBs. The use of the powder form of SEs allows the adoption of electrode materials developed for LIBs and scalable slurry-based fabrication of sheet-type electrodes and SE films. To achieve bulk-type ASLBs that show comparable performance with conventional LIBs, multiple critical challenges must be addressed. High ionic conductivity of the SEs is one of the most important issues. The modeling study by Newman and co-workers showed that electrolyte systems with a unity transference number outperformed other systems with transference number of 0.2, even when Li^+ conductivity was decreased by an order of magnitude.[28] In this regard, Li^+ conductivities for SEs in the order of 10^{-3} S cm^{-1} can compete with conventional LIBs in terms of power capabilities. However, the advantage of single-ion conducting character of SEs is often offset by difficulties in forming intimate ionic contacts with active materials in the composite electrodes.

In Figure 1b, Li^+ ionic conductivities of several representative classes of SE materials are compared with the conventional liquid electrolyte. Although LiPON material ($Li_{3.3}PO_{3.9}N_{0.17}$) was commercialized for thin-film-type ASLBs,[29,30] its low Li^+ conductivity (≈10^{-6} S cm^{-1}) prohibits the applications for bulk-type ASLBs. By the same reason, solid polymer electrolytes are also ruled out despite the advantages of lightness, flexibility, and operability with Li metal.[31–33] Several sulfide and oxide materials can satisfy the minimum requirement in Li^+ conductivity (≈10^{-4} S cm^{-1}) for room-temperature-operative ASLBs at moderate C-rates.[20] While oxide materials are superior to sulfides in terms of stability and processability at ambient environments, high-temperature sintering process is required to achieve good interfacial contacts with active materials, and accompanies deteriorating side reactions, resulting in huge cell resistances.[34,35] By contrast, since sulfide materials are mechanically sinterable at room temperature (RT), electrode–electrolyte interfacial resistances originating from their reactions during the fabrication of ASLBs can be minimized.[20,36] Moreover, the ionic conductivity of several state-of-the-art sulfide materials (e.g., LGPS,[16] $Li_7P_3S_{11}$,[37] LSiPSCl[22]) have reached that of conventional organic liquid electrolytes, implying the potential for bulk-type ASLBs to outperform conventional LIBs.

First principles computation techniques have been indispensable in the research and development (R&D) of advanced SE materials. These computational modeling techniques based on quantum mechanics have the capability of directly investigating the phenomena at the atomistic level, and have been demonstrated to be highly effective in studying ion diffusion mechanism, electrochemical stability, and interface compatibility of SE materials. Significant understandings in SE materials have been achieved based on computational studies, and rational design strategies of SEs have been established. In addition, because of the recent advancements of materials genome initiative[38] and machine learning techniques,[39] the predictive discovery and design of new SEs have also been established in first principles calculations with great successes. Multiple novel SE materials with high ionic conductivity from 10^{-4} to 10^{-2} S cm^{-1} at RT have been predicted and demonstrated.

Kern Ho Park received his B.S. degree (2011) in Korea University and Ph.D. degree (2017) from Department of Chemical and Biological Engineering, Seoul National University. His main research topics are sulfide-based solid electrolytes and electrode materials for all-solid-state batteries. Currently, he is a postdoctoral researcher in Prof. Yoon Seok Jung's group at UNIST.

Yifei Mo is an Assistant Professor of Materials Science and Engineering at the University of Maryland, College Park, USA. He received his B.S. from Peking University and Ph.D. from the University of Wisconsin-Madison, and conducted his postdoctoral research at Massachusetts Institute of Technology. His research aims to advance the understanding, design, and discovery of engineering materials through computational techniques, with current emphases on critical materials problems in beyond Li-ion and all-solid-state batteries.

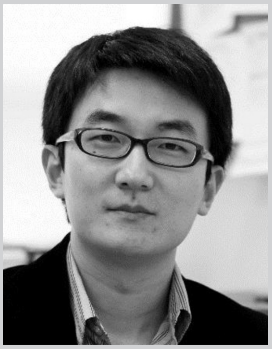

Yoon Seok Jung is an Associate Professor of Department of Energy Engineering at Hanyang University, South Korea. He received his B.S. (2001) and Ph.D. degrees (2008) in Chemical Engineering from Seoul National University, trained as an electrochemist and materials scientist, and conducted postdoctoral research (2008–2011) at University of Colorado Boulder, the University of Texas at Austin, and NREL, USA. He was an Associate Professor at UNIST, South Korea (2011–2018). His current research is focused on solid electrolytes and electrode materials for batteries.

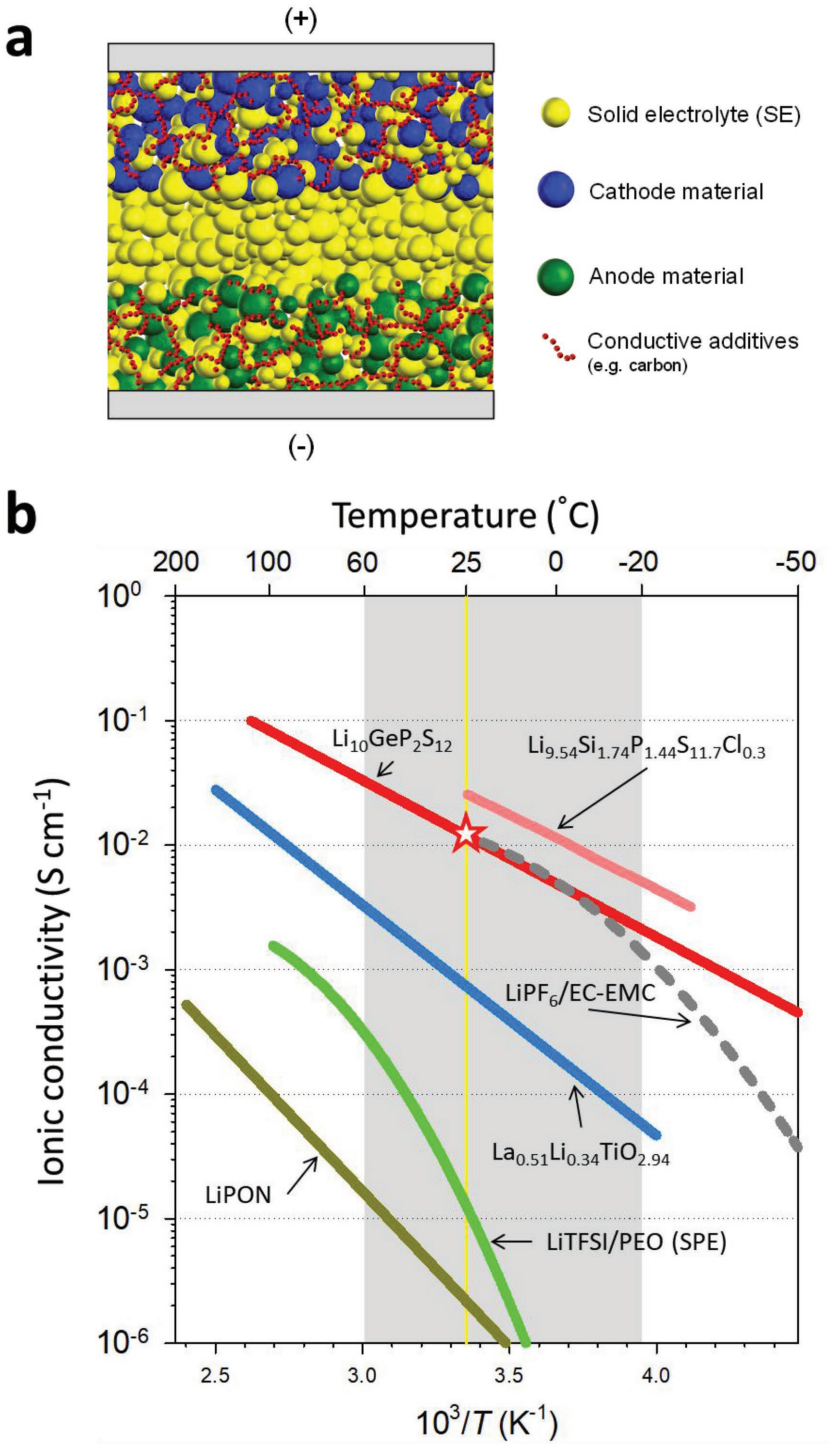

Figure 1. a) Schematic diagram of bulk-type all-solid-state batteries. Reproduced with permission.[20] Copyright 2015, Wiley-VCH. b) Arrhenius plots of Li-ion conductivities for the representative SE materials. The gray region indicates the temperature range where liquid electrolytes are stable or work.

The major R&D efforts in ASLBs using sulfide SEs to date have been focusing on improving ionic conductivity by exploring new compositions and structures. However, the explosively growing interests and the practical considerations in this field have brought about several emerging subjects, such as compatibility issues of SEs with active electrode materials, new synthesis and processing protocols for SEs, and fabrication of sheet-type electrodes. Furthermore, along with the extensive R&Ds in beyond Li-ion batteries such as Na-, K-, and Mg-ion batteries,[40–42] recent noticeable progresses in all-solid-state Na-ion batteries (ASNBs) have been made. In this progress report, we first summarize the recent advances in sulfide Li-ion SE materials regarding design strategies based on the exploration of multicomponent systems and ion transport mechanism revealed by ab initio calculations, followed by the discussions about their electrochemical stability and compatibility with active materials. Next, emerging progresses of liquid-phase synthesis and the solution process for Li-ion SEs and their prospects, especially for applications in sheet-type electrodes, are highlighted. Further, recent progresses in sulfide Na-ion SE materials and ASNBs are summarized. Finally, research directions to address the challenges and emerging issues for all-solid-state batteries using sulfide SEs are discussed.

2. Li-Ion Transport in Li-Ion SEs

2.1. Basic Considerations

In conventional carbonate-based organic liquid electrolytes, Li^+ ions are solvated preferentially by solvent molecules with high dielectric constants (e.g., ethylene carbonate), and weakly interacting linear carbonates (e.g., diethyl carbonate) smoothen the motions of Li^+–solvent complexes.[8] The net transport of Li^+ ions is driven by the difference in the chemical potential of Li^+ ions generated by charge transfer reaction at electrolyte–electrode interfaces.[43]

The ion transport mechanism in inorganic SEs is completely different in that single ion-species (such as Li^+) move through the immobile crystal structural framework. In Li-ion SEs, Li^+ ions hop between two energetically stable Li sites separated by a energy barrier through favorable migration pathways. The long-range connectivity of Li^+ sites as well as low-barrier microscopic energy landscape is essential for the fast transport of Li^+ ions. Thus, a number of factors regarding crystalline structure and materials chemistry affect the overall ionic conductivity, σ, expressed by[27,44]

$$\sigma = \frac{A}{T} n_c \exp\left(-\frac{E_a}{k_B T}\right) \quad (1)$$

where A is a constant related to the crystal structure, n_c is the concentration of mobile-ion carriers (e.g., vacancy or interstitial), E_a is the activation energy for ion transport, T is temperature in K, and k_B is the Boltzmann constant.

Equation (1) provides several important implications for improving ionic conductivity. First, an open crystal structural framework is one of the elementary prerequisites for ionic conductors. Specifically, 3D conduction pathways and large atomistic volume for ion migration pathways are desired.[45] Second, a high concentration of mobile-ion carriers, such as vacancies and interstitials, are critical: according to Equation (1), the conductivity is maximum where the mobile-ion carrier concentration n_c is optimum. For example, in the single phase $Li_{4-3x}Al_xSiO_4$ solid solution,[46] the end members, which have one particular set of Li^+ sites fully occupied (Li_4SiO_4 ($x = 0$)) and completely empty ($Li_{2.5}Al_{0.5}SiO_4$ ($x = 0.5$)), are almost insulating (<10^{-8} S cm^{-1} at >100 °C), and an optimal Li^+ conductivity is achieved at $x \approx 0.25$ (≈10^{-5} S cm^{-1}). Third, highly polarizable ions lower the migration energy barriers.[27,47,48] The sulfide SEs are more likely to achieve superionic conductivity than the oxide counterparts.[47] While the afore-discussed criteria apply to the well-defined crystal structures, the enhanced Li^+ conductivities originating from heterostructured materials are also noteworthy.[49–51] Liang found that the composite of LiI and Al_2O_3 showed a high conductivity of ≈10^{-5} S cm^{-1} at 25 °C, which was explained by the facile ion conduction in the interfacial space-charge-layer regions.[51] Large variations in Li^+ conductivities for glass and glass-ceramic sulfide SEs may also be related to complex ionic conduction at interfaces.[52–58]

2.2. Explorations of Li-Ion SEs

The initial research for sulfide Li-ion SEs in 1980s–1990s was focused on glassy materials (e.g., $Li_2S{\cdot}GeS_2$, $Li_2S{\cdot}P_2S_5{\cdot}LiI$, $Li_2S{\cdot}SiS_2$) showing conductivities in the range of ≈10^{-4} S cm^{-1} at RT.[59–65] In 2001, the first crystalline sulfide Li^+ superionic conductor, $Li_{3.25}Ge_{0.25}P_{0.75}S_4$, named as thio-lithium superionic conductor (thio-LISICON), showed higher ionic conductivity (2.2×10^{-3} S cm^{-1} at 25 °C) than conventional glassy materials. Since then, several important classes of sulfide Li^+ superionic conductors have been developed (**Table 1**): $Li_7P_3S_{11}$ (3.2×10^{-3} S cm^{-1}) in 2005,[54] an argyrodite-type Li_6PS_5X (X = Cl, Br, I, ≈10^{-3} S cm^{-1}) in 2008,[66] $Li_{10}GeP_2S_{12}$ (LGPS, 1.2×10^{-2} S cm^{-1}) in 2011,[16] and $Li_{9.54}Si_{1.74}P_{1.44}S_{11.7}Cl_{0.3}$ (LSiPSCl, 2.5×10^{-2} S cm^{-1}) in 2016.[22]

The strategies in designing Li-ion SEs are worth considering for the exploration and developments of compositions based on multicomponent systems, as illustrated in **Figure 2**. Beginning with pseudobinary systems, the most studied system is Li_2S–P_2S_5. Among the several phases along the Li_2S–P_2S_5 tie line, Li_3PS_4 crystal structure is comprised of isolated PS_4^{3-}, and $Li_7P_3S_{11}$ has an equimolar mixture of isolated PS_4^{3-} and $P_2S_7^{4-}$, both showing high Li^+ conductivities.[37,54,55,67] Whereas the room-temperature stable γ-Li_3PS_4 shows low conductivity of only 3×10^{-7} S cm^{-1}, Li^+ conductivity of β-Li_3PS_4 is in the order of 10^{-4}–10^{-3} S cm^{-1}.[54,56–58] An even higher conductivity was achieved in $Li_7P_3S_{11}$; 3.2×10^{-3} and 1.7×10^{-2} S cm^{-1} for cold- and hot-pressed samples, respectively, which is the highest among all three-element pseudobinary systems.[37,54] It should be noted that the aforementioned SE materials are prepared by mechanical milling and the subsequent heat treatment at relatively low temperatures of 150–300 °C results in glass-ceramics.[54,58] Recently, it was revealed that variations in the conductivities of glass-ceramic Li-ion SEs originate from glassy materials that were difficult to be identified by conventional X-ray diffraction (XRD) measurements.[53] In this regard, a Li_2S-deficient $Li_4P_2S_7$,[60,68] its sulfur-deficient phase $Li_4P_2S_6$,[53,69] and Li_2S-rich Li_7PS_6[70] as a mother phase of the argyrodite-type sulfide SEs are also important despite their low ionic conductivities (≈10^{-8} – 10^{-5} S cm^{-1}). Very recently, off-stoichiometric LGPS-like-structured $Li_{9.6}P_3S_{12}$ showing 1.2×10^{-3} S cm^{-1} at 25 °C was derived.[22] Important classes of phosphorus-free pseudobinary compounds are found in the Li_2S–SnS_2 system (Figure 2). The solid-state synthesized Li_4SnS_4 exhibited low conductivities in the order of 10^{-5} S cm^{-1}.[21,71,72] The Li^+ conductivity of Li_4SnS_4 could be increased to 1.4×10^{-4} S cm^{-1} as the crystallinity became lowered by the solution process using methanol (MeOH) or water.[21,72] The SnS_2-rich layer-structured Li_2SnS_3 ($Li[Li_{0.33}Sn_{0.67}S_2]$) was identified to show the conductivity of 1.5×10^{-5} S cm^{-1}.[73] The high ionic conductivity of $Li_{0.6}[Li_{0.2}Sn_{0.8}S_2]$ ($\sigma_{NMR} = 9.3 \times 10^{-3}$ S cm^{-1} at 25 °C) was also achieved by introducing vacancies into interlayer Li^+ sites.[74]

Moving to the pseudoternary system, the Li_3PS_4-Li_4GeS_4 system on the Li_2S–P_2S_5–GeS_2 plane was an important starting point (Figure 2). The well-known thio-LISICON ($Li_{3.25}Ge_{0.25}P_{0.75}S_4$) and LGPS are along this tie line. Subsequently, more LGPS families (e.g., $Li_{10}SnP_2S_{12}$,[75] $Li_{11}Si_2PS_{12}$[76]) along the Li_3PS_4–Li_4MS_4 tie line, showing high Li^+ conductivities of >10^{-4} S cm^{-1}, have been identified. Moreover, high Li^+ ionic conductivity of 1.39×10^{-3} S cm^{-1} at 25 °C was achieved for the compound $Li_{3.833}Sn_{0.833}As_{0.166}S_4$ along the Li_3AsS_4–Li_4SnS_4 tie line on the Li_2S–As_2S_5–SnS_2 plane (Figure 2).[77] Although the practical application of this compound may be limited because of the use of extremely toxic arsenic, it suggests the research on phosphorus-free compounds, which have much better stability in air than phosphorus-containing counterparts.[21,72,77] Jung and co-workers demonstrated that the conductivity of Li_4SnS_4 was enhanced by the addition of LiI using the solution process (4.1×10^{-4} S cm^{-1} at 30 °C for $0.4LiI{\cdot}0.6Li_4SnS_4$) (Figure 2).[21] Other important classes of Li-ion SEs were identified in the Li_2S–P_2S_5–LiX (X = Cl, Br, I) system, such as the argyrodite-type Li_6PS_5X (≈10^{-3} S cm^{-1}) and the soft-chemistry-derived $Li_7P_2S_8I$ (6.3×10^{-4} S cm^{-1} at 25 °C)[78] and Li_4PS_4I (max. 1.2×10^{-4} S cm^{-1} at 25 °C).[79]

Finally, the development of state-of-the-art Li^+ superionic conductor is based on the most complex pseudoquaternary system Li_2S–P_2S_5–MS_2–LiX (Figure 2). The LSiPSCl can be considered as the double aliovalent substitutions of P^{5+} and S^{2-} in Li_3PS_4 with Si^{4+} and Cl^-, respectively. In detail, the composition of $Li_{9.84}Si_{1.74}P_{1.44}S_{12}$ is derived along the $Li_4P_2S_7$–Li_4SiS_4 tie line, and the aliovalent substitution of S^{2-} in $Li_{9.84}Si_{1.74}P_{1.44}S_{12}$ with Cl^- results in the LSiPSCl ($Li_{9.54}Si_{1.74}P_{1.44}S_{11.7}Cl_{0.3}$) (Figure 2). Alternatively, this LSiPSCl composition can also be derived along the tie line of $Li_{9.48}P_{1.44}S_{1.78}S_{12}$-LiCl (Figure 2). Since LSiPSCl has a similar structure as the LGPS, LSiPSCl can also be viewed as derivative from LGPS with full Si-to-Ge

Table 1. Li-ion SEs developed in recent years (in 2010s, including several important materials).

	Composition	Year	Structure	Conductivity [S cm^{-1}, 25 °C]	E_a [eV]	Ref.
Pseudobinary	Li_3PS_4	Early 2000s	Monoclinic (glass-ceramic)	$\approx 10^{-4}$	0.23	[214,215]
	$Li_7P_3S_{11}$	2005	Triclinic (glass-ceramic)	3.2×10^{-3} 1.7×10^{-2} a)	0.176	[54,37]
	$Li_{9.6}P_3S_{12}$	2016	Tetragonal	1.20×10^{-3} a)	0.26	[22]
	Li_4SnS_4	2012	Orthorhombic	7×10^{-5}	0.41	[71]
	Li_2SnS_3	2015	Monoclinic	1.5×10^{-5}	0.59	[73]
	$Li_{0.6}[Li_{0.2}Sn_{0.8}S_2]$	2016	Monoclinic	9.3×10^{-3} (NMR) 1.5×10^{-2} (EIS, grain)	0.17 (NMR)	[74]
	Li_3AsS_4	2014	Orthorhombic	1.31×10^{-5}	–	[216]
Pseudoternary	$Li_{3.25}Ge_{0.25}P_{0.75}S_4$	2001	Monoclinic	2.2×10^{-3} a)	0.21	[47]
	Li_6PS_5X (X = Cl, Br)	2008	Cubic (argyrodite)	$\approx 10^{-3}$	0.33–0.41	[217]
	$Li_{10}GeP_2S_{12}$	2011	Tetragonal	1.2×10^{-2}	0.25	[16]
	Li_7GePS_8	2013	Tetragonal	7×10^{-3}	0.22	[218]
	$Li_{10}SnP_2S_{12}$	2013	Tetragonal	4×10^{-3} (27 °C)	0.27 (grain) 0.60 (grain boundary)	[75]
	$Li_{11}Si_2PS_{12}$	2014	Tetragonal	–	0.20 (NMR)	[76]
	$Li_{11}AlP_2S_{12}$	2016	Orthorhombic	8.02×10^{-4}	0.26	[219]
	$Li_{3.833}Sn_{0.833}As_{0.166}S_4$	2014	Orthorhombic	1.39×10^{-3}	0.21	[77]
	$Li_{3.334}Ge_{0.334}As_{0.666}S_4$	2014	Orthorhombic	1.12×10^{-3}	0.17	[216]
	$0.4LiI{\cdot}0.6Li_4SnS_4$	2016	Glass	4.1×10^{-4} (30 °C)	0.43	[21]
	$Li_7P_2S_8I$	2015	Orthorhombic	6.3×10^{-4}	–	[78]
	Li_4PS_4I	2017	Tetragonal	max. 1.2×10^{-4}	0.37–0.43	[79]
	$80(0.7Li_2S{\cdot}0.3P_2S_5){\cdot}20LiI$	2012	Glass	5.6×10^{-4}	–	[220]
	$Li_{3.45}Si_{0.45}P_{0.55}S_4$	2014	Tetragonal	6.7×10^{-3} a)	0.27	[221]
	$Li_7P_{2.9}S_{10.85}Mo_{0.01}$	2017	Triclinic	4.8×10^{-3}	0.235	[145]
	$(Li_2S)_9(P_2S_5)_3(Ni_3S_2)_1$	2017	Orthorhombic	2.0×10^{-3}	0.297	[222]
Pseudoquaternary	$Li_{9.54}Si_{1.74}P_{1.44}S_{11.7}Cl_{0.3}$	2016	Tetragonal	2.5×10^{-2} a)	0.24	[22]
	$Li_7P_{2.9}Mn_{0.1}S_{10.7}I_{0.3}$	2017	Triclinic	5.6×10^{-3}	0.216	[144]
	$Li_{10.35}[Sn_{0.27}Si_{1.08}]P_{1.65}S_{12}$	2017	Tetragonal	1.1×10^{-2} a)	0.20	[222]

a) Measured using annealed pellet.

substitution and a minor Cl-to-S substitution charge-balanced by a minor Li concentration change.

Despite the significant progresses in enhancing ionic conductivities, a critical hurdle for the practical applications of sulfide Li-ion SEs is their stability in the ambient atmosphere.[21,80] Conventional phosphorus-containing sulfide SE materials such as Li_3PS_4 show poor stability in air (against both moisture and oxygen), which can be explained by high oxygen affinity of P^{5+}.[21,72,77,81,82] One possible remedy is a partial substitution of S^{2-} with O^{2-}. For example, $xLi_2O \cdot (100 - x)(0.7Li_2S \cdot 0.3P_2S_5)$ glasses showed no H_2S evolution within 10 min upon exposure to ambient air.[83] It was also shown that the addition of FeS and basic metal oxides can suppress the H_2S evolution.[84] A more radical approach is the exclusion of phosphorus. It was demonstrated that $Li_{3.833}Sn_{0.833}As_{0.166}S_4$ and glass $LiI \cdot Li_4SnS_4$, which were developed as a branch of Li_4SnS_4,[21,77] showed excellent stability in dry air.[21,69,72,77]

2.3. Transport Mechanism and Design Strategy for Li-Ion SEs

The first step toward the rational design strategy of new SEs is to understand the Li^+ transport mechanism in these materials and the origin of their exceptionally high Li^+ conductivity. First principles computations based on ab initio molecular dynamics (AIMD) simulations and nudged-elastic-band (NEB) calculations have been demonstrated in studying the atomistic Li^+ diffusion mechanisms.[19,85–87] Many Li superionic conductor materials, such as LGPS,[85,86] β-Li_3PS_4,[88,89] and cubic phase $Li_7La_3Zr_2O_{12}$ (LLZO),[90] exhibit highly disordered Li sublattice, where a large fraction of Li sites are vacant for Li^+ hopping from neighboring sites, corresponding to a high carrier concentration n_c in Equation (1). As pioneered and demonstrated by Mo et al., AIMD simulation techniques have significant advantages in studying complex diffusion mechanisms in these Li superionic conductor SE materials.[85] Their study confirmed the fast Li^+ diffusion in LGPS and revealed the anisotropic 3D

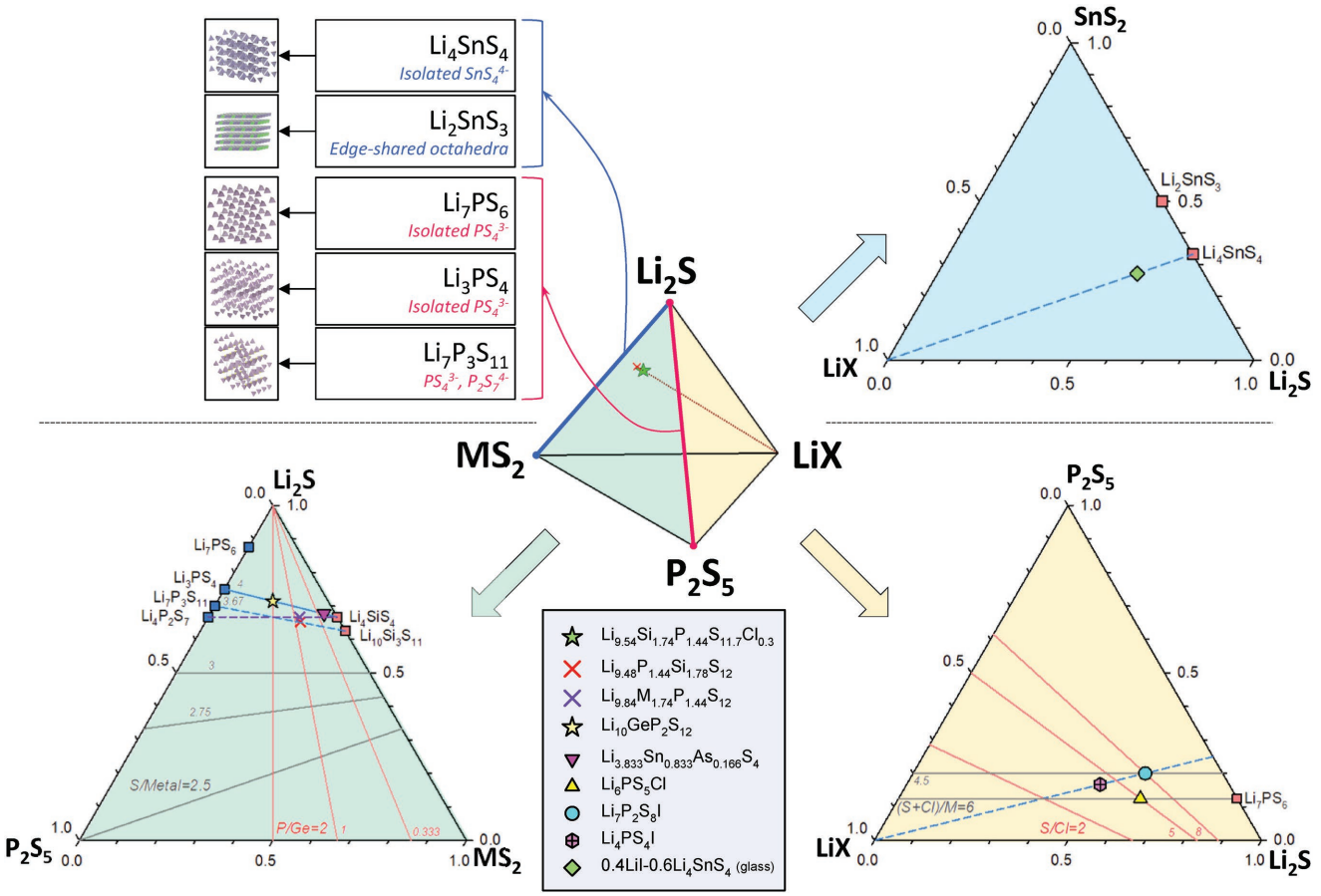

Figure 2. Pseudoquaternary diagram of the Li_2S–P_2S_5–Li*X*–MS_2 system for Li-ion SEs.

Li^+ diffusion mechanism in LGPS structure with fast 1D diffusion along the *c* direction and slower Li^+ diffusion in the *ab* plane (**Figure 3**a,b), as later confirmed by multiple experimental studies.[91–93] AIMD simulation studies of other Li sulfide SEs, such as $Li_7P_3S_{11}$[94] and argyrodite Li_6PS_5Cl,[95] confirmed their exceptionally fast Li-ion diffusion in bulk phases. In addition to these AIMD simulation studies, which quantified the overall diffusional properties, static first principles studies including NEB calculations have also been performed on Li sulfide SEs, such as Li_3PS_4, Li_4GeS_4, Li_4SnS_4, and Li_3AsS_4, to investigate the formation energies of mobile Li^+ vacancies and interstitials, Li^+ site energies in the structures, and Li^+ migration energy barriers.[73,96–98]

In addition, first principles computations were performed to predict aliovalent doping and substitution in these known materials systems to further increase Li^+ conductivity. For example, computations predicted S-to-halogen doping in Li_6PS_5Cl to create Li^+ excess with increased Li^+ conductivity.[95] Moreover, various compositions are predicted through the substitution of known compounds. For example, Si- and Sn-substituted LGPS, such as $Li_{10}SiPS_{12}$ and $Li_{10}SnPS_{12}$, were initially predicted in first principles computation (Figure 3c)[86] and then verified by multiple experimental syntheses and measurements.[22,75,76] Ong and co-workers expanded such substitution strategy into wider chemical spaces such as the Ag-P-S and Ag-*M*-P-S compositions and predicted a number of novel compounds, such as $Li_3Y(PS_4)_2$ and $Li_5PS_4Cl_2$, with Li^+ conductivity of $>10^{-3}$ S cm^{-1} at RT.[99]

Moreover, based on first principles computational studies, the general design principles for the crystal structural framework of superionic conductors were established. Ceder and co-workers identified the body-center cubic (bcc) packing of anion (e.g., S^{2-}) in the crystal structure, as found in LGPS and $L_7P_3S_{11}$, exhibits a low energy landscape for Li^+ migration (Figure 3d).[19] In bcc anion packing, Li ions occupy and migrate between face-sharing tetrahedral sites, leading to a low migration barrier of ≈0.2 eV in typical Li sulfides (Figure 3d). This general design principle has been applied to discover the materials with bcc anion framework leading to low Li^+ migration barrier. New Li sulfide SEs based on the bcc anion framework, such as $LiZnPS_4$, were discovered, and the derived $Li_{1+2x}Zn_{1-x}PS_4$ compounds are predicted to achieve high Li^+ conductivity of $>10^{-2}$ S cm^{-1} at RT.[100]

In addition to crystal structural features, Mo and co-workers uncovered that Li superionic conductors in sulfides and oxides exhibit a unique diffusion mechanism that is distinctive from typical solid materials,[87] through directly observing the real-time dynamics of Li^+ migrations during AIMD simulations. In superionic conductors, multiple Li ions migrate simultaneously through a concerted mechanism instead of an isolated ion hopping in typical solids (Figure 3e). Owing to Li^+ occupancy of high-energy sites in these Li-stuffed structures and strong Li–Li

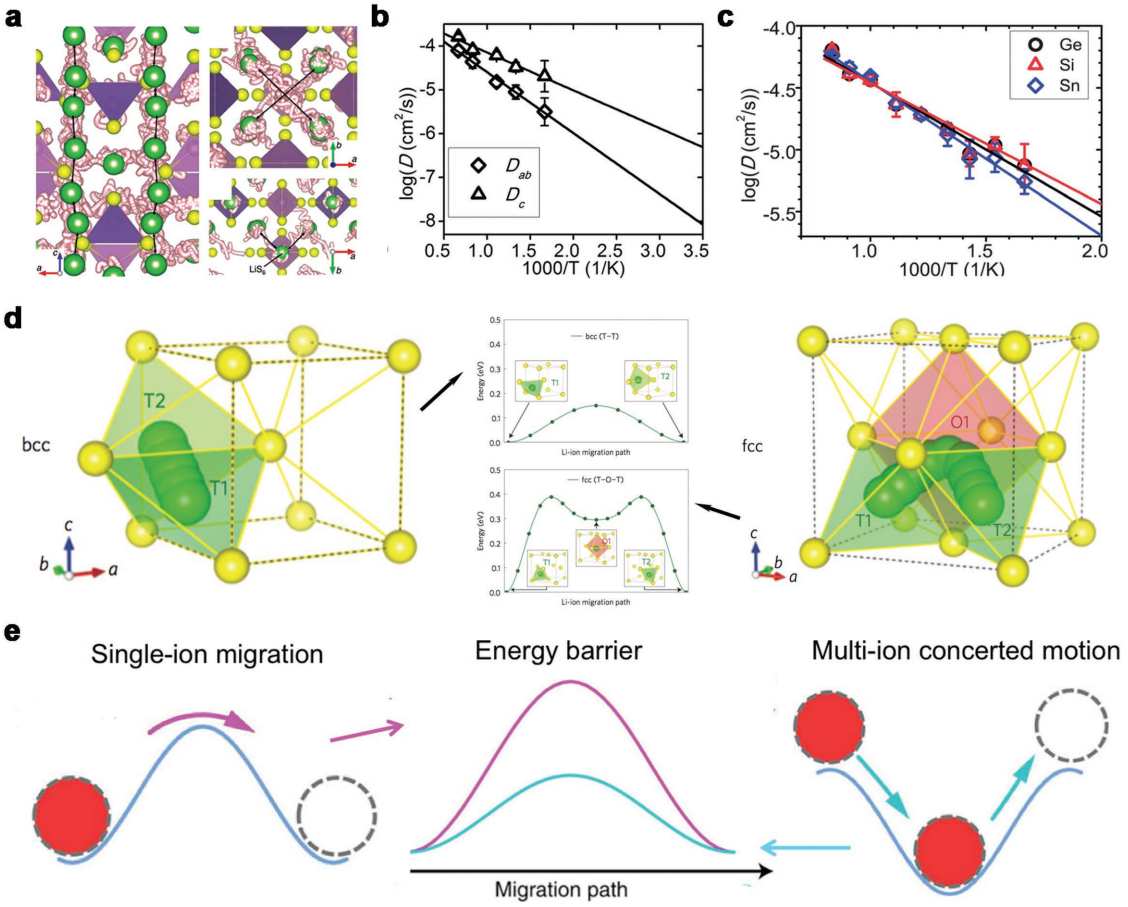

Figure 3. a) Li^+ diffusion pathway in LGPS shown by Li^+ trajectories from AIMD simulations. b) Arrhenius plots of diffusion coefficient D_c along the *c* direction and D_{ab} in the *ab* plane for LGPS from AIMD simulations. Reproduced with permission.[85] Copyright 2011, the American Chemical Society. c) Arrhenius plots of $Li_{10}MP_2S_{12}$ (M = Ge, Si, and Sn) from AIMD simulations. Reproduced with permission.[86] Copyright 2012, the Royal Society of Chemistry. d) Li^+ migration pathway and energy barrier in bcc- and face-center cubic (fcc)-type sulfur anion lattices. Reproduced with permission.[19] Copyright 2015, Nature Publishing Group. e) Schematic illustration of single-ion migration and multi-ion concerted migration with different migration energy barriers. Reproduced with permission.[87] Copyright 2017, Nature Publishing Group.

Coulomb interactions, the concerted migration with a decreased migration barrier is kinetically favorable, as the downhill Li^+ migration partially cancels out the uphill climbing of other Li^+ migration (Figure 3e). Based on the fundamental understanding of low-barrier concerted migration, Mo and co-workers proposed a general design strategy of inserting Li^+ into the high-energy sites of the structure to activate concerted migration, to significantly decrease activation energy, and to increase Li^+ conductivity. Using this design strategy, they discovered a number of new fast Li-ion conductors such as $LiTaSiO_5$ and $LiAlSiO_4$ with predicted RT Li^+ conductivity of $>10^{-3}$ S cm^{-1} at the optimal doping concentrations.[87] Therefore, first principles computation methods have been demonstrated with strong capabilities in discovering and designing new SEs materials.

3. Electrochemical Stability and Interface Compatibility of Li-Ion SEs

To achieve the optimal electrochemical performances of ASLBs, the operating voltage of electrodes should be within the range of stability window of SEs or stable passivating interfaces should be formed between the SE and electrodes. Contrary to the naive belief that the electrochemical stability window of inorganic SEs would be much wider than that of liquid electrolytes, recent theoretical and experimental studies on electrode–SE interfaces have revealed narrow thermodynamic electrochemical stability windows for SEs (**Figure 4**a) and dynamic evolutions at electrode–SE interfaces upon charge and discharge.[58,101–104] Accordingly, it has been shown that the electrochemical performances of ASLBs are significantly affected not only by ionic conductivity but also by the electrochemical stability and interface compatibility of SEs.[58] Upon typical operation voltage ranges of all-solid-state batteries, the SEs are subjected to decomposition, forming byproducts as interphase layers. If the formed layers are mixed ionic and electronic conducting (MIEC), the decomposition would propagate into the bulk of the SE (Figure 4b). If the layers are electronically insulating but ionically conducting, as the solid electrolyte interphase (SEI) layers in conventional LIBs, the interphase layers would remain stable (Figure 4b), which is desired for ASLBs. It is also important that chemical reactions between

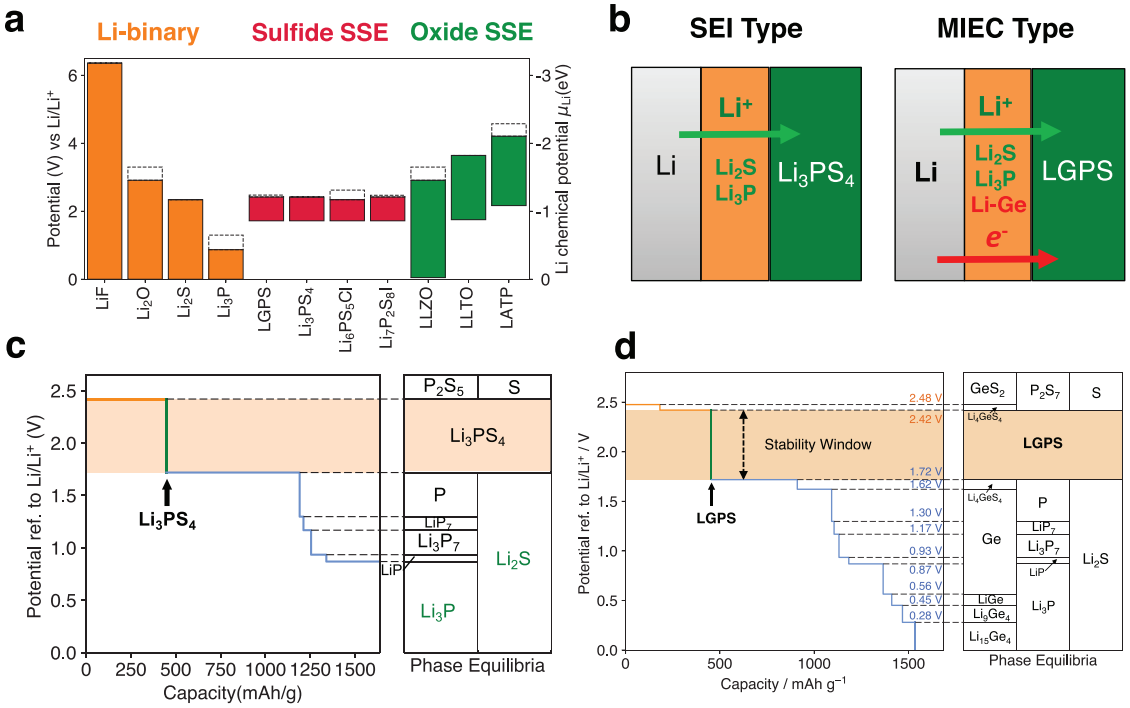

Figure 4. a) Electrochemical stability of common SEs and Li binaries. Reproduced with permission.[107] Copyright 2015, the American Chemical Society. b) Schematic illustration of interphase layer of Li_3PS_4 and LGPS against Li metal with different conducting properties and interface compatibility. Equilibrium voltage profiles of c) Li_3PS_4 and d) LGPS with corresponding phase equilibria. Reproduced with permission.[108,109] Copyright 2016–2017, Wiley-VCH.

partially charged electrodes and SEs are possible,[105,106] which leads to severe degradation of ASLBs upon prolonged storage and uses. Therefore, understanding and controlling the interfacial chemistries between electrodes and SEs are critical to the development of high-performance ASLBs.

3.1. Intrinsic Electrochemical Window of SEs

First principles calculations were performed to identify the electrochemical windows of the aforementioned sulfide SE materials.[101,107,108] Based on the thermodynamic data from first principles calculations, the critical potentials were identified for the onset of thermodynamically favorable reduction (lithiation) or oxidation (delithiation) of the SEs, and the range between these two critical potentials gives the electrochemical window. As shown by first principles computation,[101,107,108] lithium thiophosphate-based SEs have a narrow thermodynamic intrinsic electrochemical window of ≈1.7–2.5 V (vs Li/Li$^+$) (Figure 4a), because of the high reduction potential of P^{5+} and the low oxidation potential of S^{2-} in the thio-phosphate chemistry. This narrow window is general among most of these Li sulfide SEs for a range of cation, anion, structure, or doping (Figure 4a). In comparison, Li binaries, such as LiF, Li_2O, Li_2S, and Li_3P, are thermodynamically stable against Li metal, because of the absence of non-Li cation that is subjected to reduction at low potentials. The thermodynamic intrinsic stability windows of sulfide SEs are significantly narrower than known oxide SEs, such as Li garnet LLZO and NASICON $Li_{1.3}Al_{0.3}Ti_{1.7}(PO_4)_3$ (LATP) (Figure 4a). In particular, Li garnet LLZO shows better stability against Li metal, and NASICON LATP shows high oxidation potential.

3.2. SE–Anode Interfaces

The Li reduction behavior of the SEs also depends on different cation chemistry, which can lead to different interphase formations and different interface compatibilities.[107,109] For example, as predicted by first principles thermodynamic calculations, the reduction of P in Li_3PS_4 starting at 1.7 V leads to the formation of lithiated products Li_3P and Li_2S on Li metal or at 0 V (vs Li/Li$^+$) (Figure 4c). Other SE materials in this Li–P–S system, such as $Li_7P_3S_{11}$ and $Li_2S{\cdot}P_2S_5$ glass, have similar voltage profiles and lithiation products. The limited electrochemical stability windows of sulfide Li-ion SEs and their dynamic evolutions at the SE–electrode interfaces were also observed and confirmed in experiments. The formation of Li_3P and Li_2S as the interphase layers of these SEs on Li metal is confirmed by in situ X-ray photoelectron spectroscopy (XPS) experiments.[103] The interphase layer consisting of Li_3P and Li_2S, which are poor electronic conductors, is passivating. Therefore, many lithium thiophosphate compounds are observed to be Li metal compatible in experiments, as the reactions at the Li–SE interface are self-limiting (Figure 4b). By contrast, from the same first principles thermodynamic analyses,[108] LGPS shows a similar electrochemical window but different Li reduction behavior compared to the materials based on the Li–P–S system. The key difference is the reduction of Ge and Li–Ge alloying reaction at <0.6 V leading to the formation of MIEC interphase

layer and poor interface compatibility (Figure 4d). The formation of Li–Ge alloys at the interfaces on Li metal has also been confirmed by in situ XPS experiments.[110] As Li–Ge alloys are good electronic conductors, the MIEC interphase layer allows the simultaneous transport of Li^+ and e^- and favorable Li reduction (Figure 4b). As a result, the interphase layer thickness and interfacial resistance grow over a short period of time.[110] This interface mechanism explains the reduction of LGPS observed at <0.6 V (vs Li/Li^+) in cyclic voltammetry (CV) experiments (**Figure 5**a), compared to the absence of major reduction peak of Li_3PS_4 down to 0 V.[58]

3.3. SE–Cathode Interfaces

At the cathode side, the potential of commonly used oxide cathode materials is beyond the anodic limit of these sulfide SEs (Figure 4a).[58,107,108] The oxidation products of Li sulfide SEs may mostly be electronically insulating and hence passivating (Figure 4c,d), which explains the higher oxidation potential than the thermodynamic intrinsic window observed in the CV measurements (Figure 5a).[58,108] However, the reactions of sulfide SEs with oxide cathodes are a critical problem causing poor SE–cathode interface compatibility. First principles calculations found that the reactions between Li sulfide SEs and oxide cathodes are highly favorable, which leads to the spontaneous formation of transition metal sulfides.[101,102] For example, first principles computation indicates that Li_3PS_4 reacts highly exothermically with $LiCoO_2$ and forms cobalt sulfides.[101,102,106,111] These transition metal sulfides are electronically conductive, leading to nonpassivating MIEC interphase layers and poor interface compatibility. The visualization of the $LiCoO_2$–$Li_2S \cdot P_2S_5$ interfaces was carried out by transmission electron microscopy (TEM) analysis (Figure 5b), by which the mutual diffusion of Co, P, and S at the interface was demonstrated.[106] More detailed chemical information of the interfacial layers was obtained by postmortem XPS.[112] Figure 5c displays the XPS spectra for $LiCoO_2$–Li_6PS_5Cl electrodes before and after the cycles. The analyses of S 2p, P 2p, and Li 1s spectra suggested the formation of elemental sulfur, polysulfides, P_2S_x species (x >5), and LiCl as the oxidative decomposition product for Li_6PS_5Cl while phosphates (PO_4^{3-}) were formed on the surface of $LiCoO_2$. Consistently, the phosphates (PO_4^{3-}) and sulfites (SO_3^{2-}) were directly detected by time-of-flight secondary ion mass spectrometry measurements of the cycled $LiNi_{0.8}Co_{0.15}Al_{0.05}O_2$–$75Li_2S \cdot 25P_2S_5$ electrode.[113] To solve this cathode interface incompatibility issue, the application of protective oxide coating layers, such as $LiNbO_3$,[21,22,114] $LiNb_{0.5}Ta_{0.5}O_3$,[115] $Li_4Ti_5O_{12}$,[116] Ta_2O_5,[117] Al_2O_3,[118] and Li_3PO_4[119] between sulfide SEs and $LiCoO_2$ was demonstrated in previous experiments. Computational studies confirmed the improved interface stability and compatibility from the thermodynamic perspective.[101,102,107]

3.4. Use of Multiple SEs in a Single Cell for ASLBs

In short, despite the narrow electrochemical windows of sulfide Li-ion SEs, the formation of favorable passivating layers and the use of protective coating layers enables desirable performances of ASLBs. It is important to note that the asymmetric stability of SEs is meaningful for ASLBs but is not so for conventional LIBs based on liquid electrolyte. For example, vinylene carbonate (VC) is reduced prior to the decomposition of ethylene carbonate (EC) and forms a stable SEI layer on graphite electrodes, significantly improving the performances of half-cells.[120,121] However, with regard to the full-cells, the decomposition of VC on the cathodes is parasitic, resulting in the fast increase in total cell resistances.[122–124] Lithium-bis-trifluoromethanesulfonylimide (LiTFSI) exhibits good thermal stability[125] and good electrochemical performance when used for carbonaceous anode materials,[126,127] but causes severe corrosion of Al current collectors for the cathodes.[128] In stark contrast, multiple SE materials through a multi-layer strategy can be employed in a single cell for ASLBs. This unique advantage in the design of ASLBs was demonstrated by comparing the TiS_2/Li-In all-solid-state cells using mono-layer LGPS and bilayer LGPS/Li_3PS_4 (Figure 5d).[58] The use of bilayer allowed the conductance of the SE layer to be maximized while avoiding the detrimental reaction between LGPS and Li–In.

3.5. Alternative Electrode Materials Enabled by SEs for ASLBs

The Li metal batteries, as an ultimate goal to achieve high energy density of batteries, have long been the Holy Grail for several decades, and the inorganic SEs have been regarded as the most promising enabler.[20,23,129] This hope was based on the previously overestimated electrochemical stability of SEs and the theory by Monroe and Newman that the dendritic growth of Li metal may be suppressed by employing inorganic SEs with high shear modulus.[130] However, in agreement with the suggestion by theoretical calculations,[101,102] the reduction of sulfide Li-ion SEs has been verified by in situ XPS analysis (Figure 5e).[110] It turned out that, when using Li metals, neither oxides nor sulfides inorganic SEs,[20,131,132] could avoid the internal short circuit caused by the penetrating growth of Li metal through the grain boundary and porous defects of the polycrystalline oxide and sulfide SE materials (Figure 5f).[132] The strategies to enable Li metal using SEs should aim for homogeneous current distributions by forming intimate contacts between SEs and Li metal, as well as for desirable chemical stability with Li metal.[109] It was shown that the deposition of additional thin layers of Au or In by vacuum evaporation, which covered voids and grain boundaries on the surface of SEs in bulk-type ASLBs, could enable the reversible deposition/stripping of Li metal in ASLBs.[133–135] This is also consistent with the significantly enhanced interfaces of oxide SE–Li metal by the ultrathin Al_2O_3 coating layer obtained by atomic layer deposition.[136] The coatings of Li-metal compatible SEs (e.g., $LiI \cdot Li_4BH_4$) were shown to enable Li metal.[77] Despite the afore-described progresses, fair evaluation on the usage of thin SEs (<100 μm) is still required for practical ASLB applications.

High-capacity cathode materials, such as S and Li_2S, are also considered for ASLBs owing to the absence of polysulfides dissolution problem.[20,137–140] In addition, first principles computation also suggests interface compatibility between sulfides SEs with S/Li_2S and sulfide cathode (e.g., $LiTiS_2$), which are

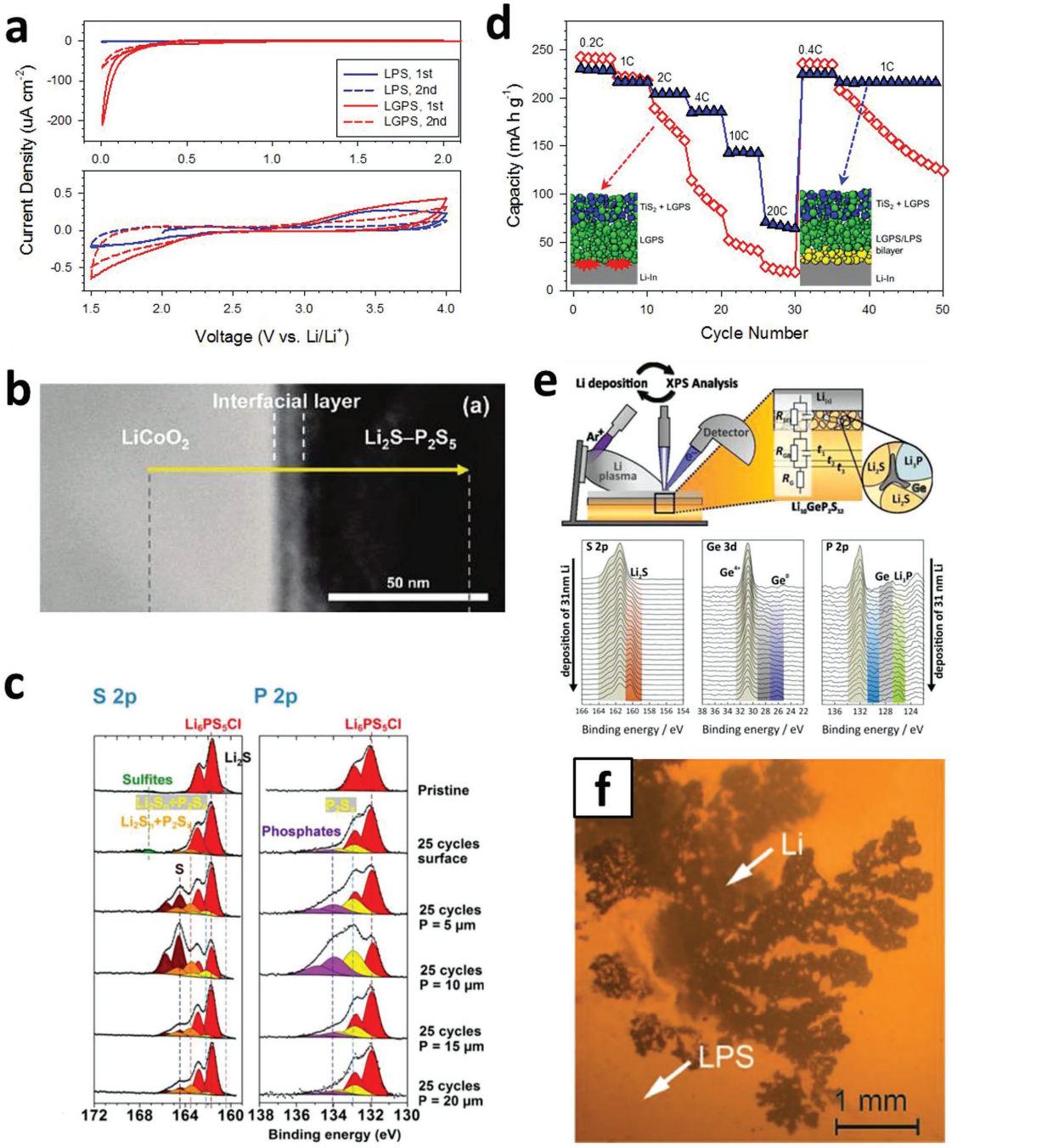

Figure 5. Results of electrochemical stability and interface compatibility for Li-ion SEs. a) First two CV cycles of Ti/Li_3PS_4/Li-In and Ti/LGPS/Li-In cells in the negative and positive potential ranges. Reproduced with permission.[58] Copyright 2014, Elsevier. b) Cross-sectional high-angle annular dark field (HAADF) STEM image of $LiCoO_2$–Li_2S·P_2S_5 interface after initial charging. Reproduced with permission.[106] Copyright 2016, the American Chemical Society. c) XPS spectra of the composite $LiCoO_2$ electrode for $LiCoO_2$/Li_6PS_5Cl/Li–In cells before and after cyclings. Reproduced with permission.[112] Copyright 2017, the American Chemical Society. d) Variations in charge capacities versus cycle number for the TiS_2/Li–In all-solid-state cells cycled at different rates between 1.5 and 3.0 V (vs Li/Li$^+$). Reproduced with permission.[58] Copyright 2014, Elsevier. e) Schematic diagram illustrating in situ XPS revealing the chemical reaction at the Li/LGPS interfaces and the corresponding XPS spectra recorded during deposition of Li metal on LGPS. Reproduced with permission.[110] Copyright 2016, the American Chemical Society. f) Transmission optical microscopy image showing penetration of Li metal into cold-pressed polycrystalline β-Li_3PS_4. Reproduced with permission.[132] Copyright 2016, Wiley-VCH.

essential for good ASLB performance.[102,105] However, the critical drawbacks of S/Li_2S electrode, such as poor electronic and ionic conductivities along with large volume changes upon discharge and charge, still remain for the ASLB applications. The low operating voltages (≈2.1 V vs Li/Li$^+$) for S (or Li_2S) are advantageous for electrochemical stability and interface

compatibility but is a major limitation for high energy density. Various preparation methods, such as ball-milling,[137,141–146] wet method,[147,148] and gas-phase mixing[139] have been applied to prepare the Li_2S (or S) composites with SEs and carbon additives, achieving reversible capacities ranged from 220 to 830 mA h (g of Li_2S)$^{-1}$.[20,137,141,143] Recently, Wagemaker and co-workers revealed that Li-ion transport across the SE–Li_2S interface rather than within the SE itself is a major kinetic limitation, by probing Li_2S–Li_6PS_5X (X = Br, Cl) using 2D-exchange nuclear magnetic resonance (NMR) spectroscopy (2D-EXSY).[143,149]

4. Wet Synthesis and Solution Process of Li-Ion SEs

For the preparation of sulfide SEs, conventional synthesis protocols for ceramic materials, such as high-temperature solid-state reaction, mechanochemical method, and melt-quenching method, have been commonly applied (**Figure 6**). Recently, the first report of wet-chemical synthesis of β-Li_3PS_4 using tetrahydrofuran (THF) at low temperatures has opened new opportunities in this field in several perspectives.[150] First, the wet-chemical synthesis of SEs may offer advantages in the mass production of SEs by reducing processing time and efforts for mixing precursors. Second, the size and morphology of the SE particles can be controlled by the wet chemistry of SEs, which affect the microstructure of electrodes and in turn the electrochemical performances.[151] Third, recent reports suggest that soft chemistry provides an access route to obtain new metastable materials that may not be possible using conventional synthesis protocols.[78,79,150] Finally, it has been demonstrated that a few optimal combinations of SEs and solvents that form homogeneous solutions without side reactions can be applied to mitigate the poor ionic contact problem in ASLB electrodes,[21,72,81,82,152,153] which are discussed in detail in Section 5.

The protocols for the preparation of SEs using solvents can be classified into two: "liquid-phase synthesis" and "solution process," as illustrated in Figure 6. For the liquid-phase synthesis, after SE precursors of Li_2S and P_2S_5 are added into solvents, forming inhomogeneous solutions composed of intermediate solid products and supernatant, wet-chemical reaction proceeds. By contrast, for the solution process, SEs, rather than precursors, are dissolved in solvents, forming homogeneous and transparent solutions. The following processes for both cases are the same: evaporation of solvents and the subsequent heat-treatment.

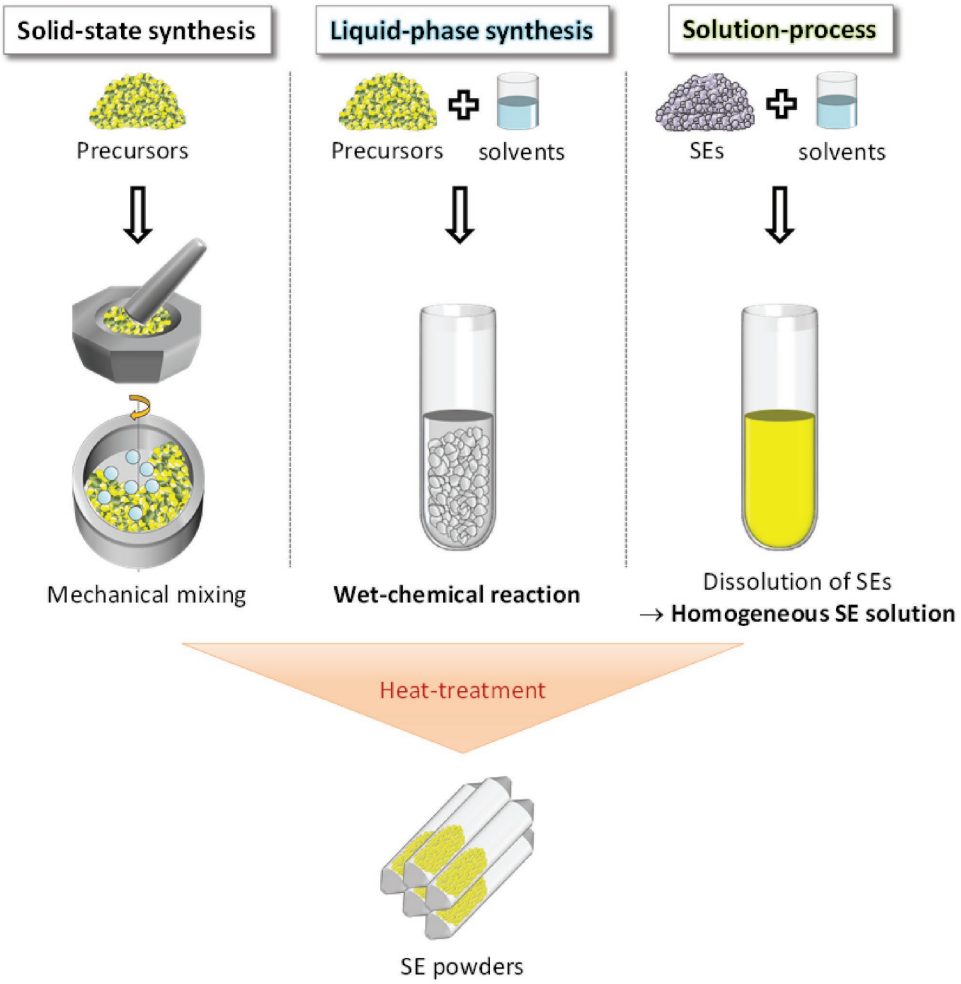

Figure 6. Schematic diagram illustrating preparation of sulfide SE materials by the conventional solid-state methods, the liquid-phase synthesis, and the solution process.

4.1. Liquid-Phase Synthesis of SEs

In the first report of liquid-phase synthesis of sulfide SEs by Liang and co-workers, β-Li_3PS_4 was prepared by adding Li_2S and P_2S_5 into THF.[150] The formation of SE-solvent complex $Li_3PS_4 \cdot 3THF$ was confirmed after the removal of liquids. The subsequent heat-treatment at 140 °C resulted in the formation of nanoporous β-Li_3PS_4, showing a high conductivity of 1.6×10^{-4} S cm^{-1} at 25 °C. It was noted that this value was higher than the one prepared by conventional solid-state reaction.[56,57] Importantly, the benefit of wet-chemistry-derived nanostructure for β-Li_3PS_4 on the abnormally high conductivity was highlighted. The following researches to obtain Li_3PS_4 were conducted using various solvents such as ethyl acetate[154] and ethyl propionate,[151] in which slightly enhanced ionic conductivities of 3.3×10^{-4} and 2.0×10^{-4} S cm^{-1} were reported, respectively. In addition, $Li_7P_3S_{11}$ was derived by wet-chemical synthesis using THF,[155] dimethoxyethane (DME),[156] and acetonitrile (ACN),[155,157] resulting in high conductivities up to 9.7×10^{-4} S cm^{-1}. A detailed summary of the wet-chemical syntheses of sulfide Li-ion SEs and their corresponding ionic conductivities are summarized in **Table 2**.

It is important to note that the size of SEs prepared by wet-chemical routes can be decreased to nanometer ranges,[150,151] while those prepared by solid-state reactions are greater than 10 μm.[21] For ASLB electrodes, larger-area ionic contacts between active materials and SEs with smaller volume fraction of SEs are desired. In this regard, the small particle size of SEs derived by liquid-phase synthesis is desired to achieve the high energy density of ASLBs. Moreover, recent reports suggest that liquid-mediated reactions could provide synthetic routes for a new class of ionic conductors.[78,79,150] $Li_7P_2S_8I$ (6.3×10^{-4} S cm^{-1} at 25 °C)[78] and Li_4PS_4I (1.2×10^{-4} S cm^{-1} at 25 °C)[79] exhibiting unprecedented crystal structures were obtained by the soft-chemistry approach using ACN and DME, respectively. Tadanaga and co-workers demonstrated that the rapid formation of PS_4^{3-} units was enabled by ultrasonic irradiation for the preparation of $Li_7P_3S_{11}$ (1.0×10^{-3} S cm^{-1} at 22 °C) using ACN.[158]

Despite the afore-described progresses, new liquid-phase chemistries remain to be unveiled. Simple criteria for selection of proper solvents for the liquid-phase synthesis of sulfide SEs are available at the current stage; functional groups that interact with the SE precursors but should not be decomposed, and low boiling points to minimize energy in the process. Very recently, Liu and co-workers reported a two-step formation mechanism of $Li_7P_3S_{11}$ in ACN: the liquid-phase reaction proceeds, resulting in $Li_3PS_4 \cdot ACN$ precipitates and soluble $Li_2S \cdot P_2S_5$, and crystalline $Li_7P_3S_{11}$ is formed by subsequent solid-state reaction.[159] Elucidating the mechanism of these complex chemistries would guide further progress.

4.2. Solution-Processable SEs

The solution processability of SEs allows harvesting the most notable advantage of using liquid electrolytes, i.e., the excellent wettability. The homogenous SE solutions can wet any surfaces

Table 2. Wet-synthesized and processed sulfide SEs.

Synthesis/Process protocol	Composition	Solvent	Conductivity [S cm^{-1}] at 25 °C	Heat-treatment temperature [°C]	E_a [eV]	Ref.
Liquid-phase synthesis	Li_3PS_4	THF	1.6×10^{-4}	140	0.356	[150]
		Ethyl acetate	3.3×10^{-4}	160	0.32	[154]
		Ethyl propionate	2.0×10^{-4}	170	0.43	[151]
	$Li_7P_3S_{11}$	DME	2.7×10^{-4}	250	0.39	[156]
		ACN	9.7×10^{-4}	250	0.323	[155]
		ACN (ultrasonication)	1.0×10^{-3} (22 °C)	220	0.132	[158]
		THF	2.3×10^{-4}	250	0.362	[155]
	$Li_7P_2S_8I$	ACN	6.3×10^{-4}	200	–	[78]
	Li_4PS_4I	DME	1.2×10^{-4}	200	0.37	[79]
	Na_3SbS_4	Water	$(1–2) \times 10^{-4}$	200	–	[190]
Solution process	$Li_{3.25}Ge_{0.25}P_{0.75}S_4$	Anhydrous hydrazine	1.82×10^{-4} (30 °C)	240	0.42	[160]
	$80Li_2S \cdot 20P_2S_5$	NMF	2.6×10^{-6}	150	0.44	[161]
	Li_3PS_4	NMF	2.3×10^{-6}	180	0.47	[162]
	Li_6PS_5Cl	EtOH	1.4×10^{-5}	80	0.34	[153]
	Li_6PS_5Br	EtOH	1.9×10^{-4}	150	0.38	[165]
		Ethyl propionate-EtOH (sonication)	3.4×10^{-5}	180	–	[223]
	$0.4LiI \cdot 0.6Li_4SnS_4$	MeOH	4.1×10^{-4} (30 °C)	200	0.43	[21]
	Li_4SnS_4	Water	1.4×10^{-4} (30 °C)	320	–	[72]
	Na_3SbS_4	MeOH or water	$(1–2) \times 10^{-4}$	100–200	0.30-0.38	[81]
	$Na_{3.75}Sn_{0.75}Sb_{0.25}S_4$	Water	2×10^{-4} (30 °C)	550	–	[82]

of active materials and infiltrate tortuous porous structures of composite electrodes in ALSBs. To date, only a few combinations of SE/solvents for solution-processable SEs have been demonstrated (Table 2). Thio-LISICON ($Li_{3.25}Ge_{0.25}P_{0.75}S_4$) was obtained using anhydrous hydrazine, showing a high conductivity of 1.82×10^{-4} S cm^{-1} at 30 °C.[160] However, its practical application was inhibited by the use of highly toxic and dangerously unstable anhydrous hydrazine. Li_3PS_4 was shown to be precipitated from the homogeneous solution using *N*-methyl formamide (NMF).[161,162] Unfortunately, the resulting Li^+ conductivity was too low (2.6×10^{-6} S cm^{-1} at 25 °C), and the solvent is difficult to be removed because of its high boiling point (≈183 °C). Ethanol (EtOH) was demonstrated to fully dissolve the argyrodite SEs Li_6PS_5X and to evaporate, resulting in the original crystals with high Li^+ conductivities of $\approx 1 \times 10^{-4}$ S cm^{-1} maximum, under low heat-treatment temperature (≤200 °C).[152,153] This is not anticipated, considering that PS_x species are vulnerable to hydrolysis or alcoholysis reactions with protic solvents such as water and alcohol, which results in the evolution of H_2S.[80] Although Li_2S is also hydrolyzed to form H_2S upon exposure to water,[80] it can be dissolved into anhydrous EtOH without side reactions.[163,164] It is postulated that the dissolved Li_2S in EtOH might decrease the proton activity of EtOH, thus suppressing the alcoholysis of PS_x^{y-} species in the Li_6PS_5X-EtOH solution. The two-step solution process for Li_6PS_5X in a previous report could be rationalized in this context; the Li_2S-EtOH solution was prepared prior to mixing with Li_3PS_4-THF solution.[165]

Another important breakthrough in solution-processable SEs was achieved in the course of searching phosphorus-free materials. Li_4SnS_4 can be fully dissolved into water with negligible H_2S evolution, which is sharply contrasted by severe hydrolysis and the subsequent intensive H_2S evolution for Li_3PS_4.[72] Moreover, Li_4SnS_4 is solution-processable using MeOH without suffering from side reaction.[21] This can be explained by the less affinity of O^{2-} with Sn^{4+} than with P^{5+}, following the hard and soft acid and base theory.[21,72,77,81,82] The recrystallization of the homogeneous aqueous Li_4SnS_4 solution resulted in preserved crystalline structure with a high Li^+ conductivity of 1.4×10^{-4} S cm^{-1} at 30 °C.[72] The incorporation of LiI into the Li_4SnS_4–MeOH solution further raised the ionic conductivity to 4.2×10^{-4} S cm^{-1}.[21] It is also noted that the resulting $LiI \cdot Li_4SnS_4$ is amorphous, and shows more softness than crystalline Li_4SnS_4, which could not be obtained by conventional synthetic protocols.[21]

Similar to the Li-ion SEs, the first solution-processable Na-ion SEs were developed for phosphorus-free materials, Na_3SbS_4[81] and $Na_{4-x}Sn_{1-x}Sb_xS_4$,[82] which are discussed in detail in Section 6.

5. Electrodes

The developments of state-of-the-art SEs such as LSiPSCl (25 mS cm^{-1}) showing even higher Li^+ conductivity than that of conventional liquid electrolytes (≈10^{-2} S cm^{-1}) indicate the superior performance of ASLBs than conventional LIBs because SEs may potentially avoid the issues of concentration polarization and desolvation processes occurring in liquid electrolytes.[22,23,166,167] Kanno and co-workers successfully demonstrated the ASLBs outperforming conventional LIBs in terms of power capabilities and operational temperature ranges. The ASLBs employing LSiPSCl or LGPS outperformed LIBs over a wide temperature range from −30 °C to 100 °C. In particular, the power densities of ASLBs at 100 °C, at which the conventional LIBs fail to work, were even superior to supercapacitors (**Figure 7**a). Moreover, the good rate capability was achieved for the high energy ASLBs using ultrathick electrodes (≈600 µm, mass loading of 115 (mg of $LiCoO_2$) cm^{-2}).[168] Through a different approach, the rate capability of ASLBs can also be boosted by applying nanostructured electrode materials,[161,169] as were the cases for the developments of LIBs.[170–172] Jung and co-workers applied TiS_2 nanosheets prepared by mechanochemical lithiation and followed by exfoliation in water under ultrasonication for ASLBs, demonstrating outstanding rate capability (Figure 7b).[169]

Layer-structured $LiCoO_2$ is the most extensively investigated electrode materials for ASLBs.[114–119] The state-of-the-art $LiCoO_2$ electrodes in lab-scale all-solid-state cells showed high discharge capacities which are close to the theoretical value (≈137 mA h g^{-1} with a cut-off voltage of 4.2 V (vs Li/Li^+)) and stable cycling performances up to 50–100 cycles.[21,115,152,168,173,174] However, the electrochemical performances are affected by several factors; resistance of SE layers,[26,58] thickness of electrodes,[168] preparation condition[173] and composition of electrode mixtures,[115,174] and pressure applied to the cells.[175]

5.1. Practical Considerations and Technical Challenges for Electrode Fabrication

One of the major R&D efforts in architecturing conventional LIB electrodes has been the electrical wiring of active materials using nanostructured conducting materials such as graphene and carbon nanotubes,[176,177] with no concern about the electrolyte wetting onto the active materials. In stark contrast, for ASLB electrodes, connecting and contacting active materials ionically are an additional technical challenge.[21,152] The porosity values of the composite electrodes for ASLBs are typically 10–20% for the electrode composition that is realistic for practical applications.[21,152] This significant amount of porosity reflects insufficient ionic contacts between SEs and active materials, limiting the full utilization of the electrodes. Besides reduced capacity, the inhomogeneity in the distributions of active materials and SEs also lowers the rate performances of ASLBs.[21,178] Moreover, while the use of carbon additives are necessary to create electric conduction pathway to active materials, these additives may also disturb intimate ionic contacts between SEs and active materials.[58,152,179] For this reason, adding too much carbon additives would result in degraded performances, in contrast to the case in conventional LIBs.[58,152,179] An extreme example was found in $LiFePO_4$, which showed negligible capacities for ASLBs (Figure 7c).[179] Jung and co-workers successfully demonstrated that the addition of the SE-compatible solvate ionic liquid LiG3, an equimolar complex of LiTFSI and triethylene glycol dimethyl ether (G3), significantly increased the capacity. The underlying mechanism was the provision of additional ionic conduction pathways by wetting the surfaces of carbon-coated $LiFePO_4$ and filling the void spaces with LiG3 (Figure 7d).

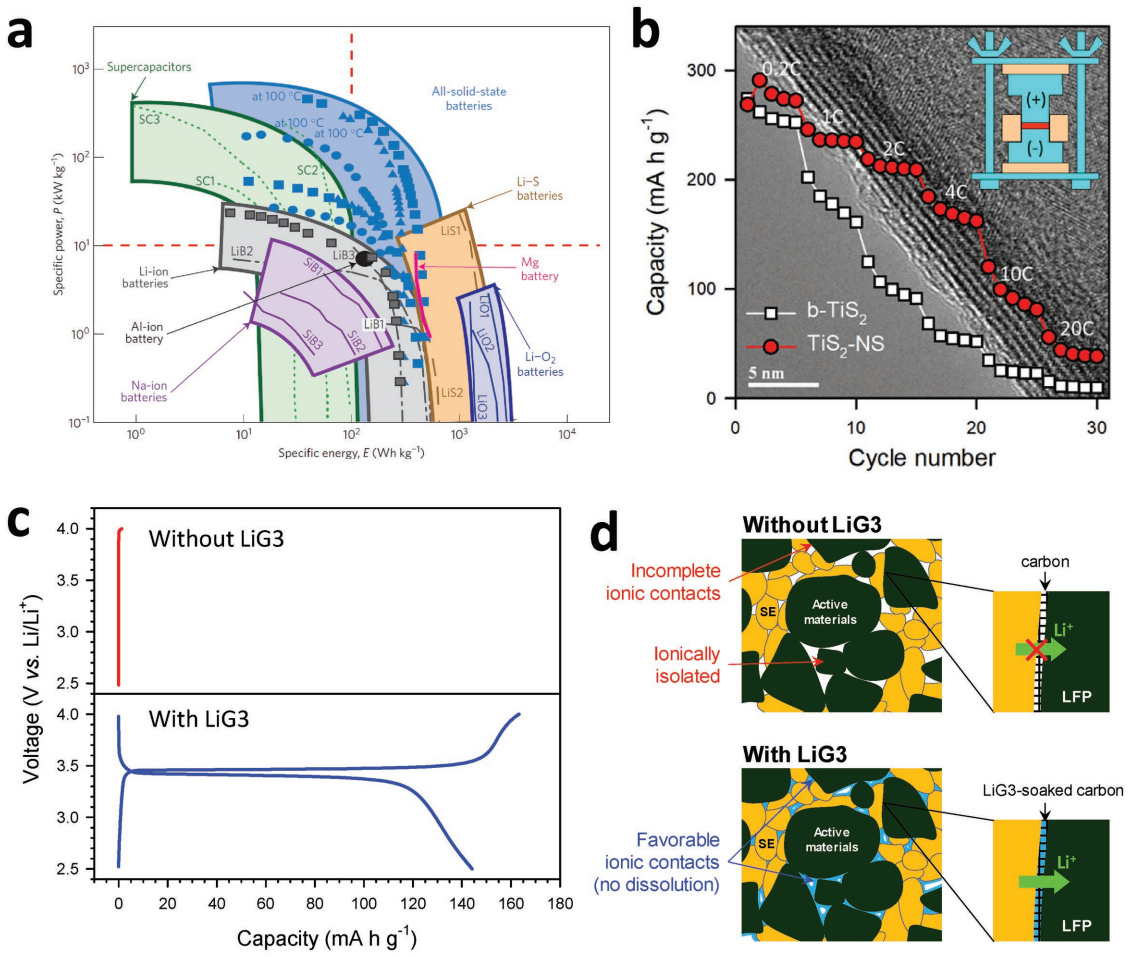

Figure 7. Electrochemical performances of ASLBs using sulfide SEs. a) The Ragone plots of ASLBs and conventional batteries and capacitors. Reproduced with permission.[22] Copyright 2016, the Nature Publishing Group. b) Rate capabilities of all-solid-state cells using bulk TiS_2 (b-TiS_2) and TiS_2 nanosheets (TiS_2-NS). Reproduced with permission.[169] Copyright 2016, the Royal Society of Chemistry. c) Second charge–discharge voltage profiles of $LiFePO_4$/Li–In all-solid-state cells without and with solvate ionic liquid, Li(G3)TFSI (LiG3), at 0.1 C. d) Schematic diagram illustrating the microstructure of the composite electrodes without and with LiG3, showing that LiG3 improves the imperfect solid–solid contacts. Reproduced with permission.[179] Copyright 2015, Wiley-VCH.

From a practical point of view, the afore-discussed promising electrochemical performances of ASLBs would depreciate if polymeric binders were not included in the composite electrodes. The conventional dry-mixed electrodes, even if they are good testing vehicles to assess the performances of electrode materials and SEs, would be difficult to scale up because of their fragile properties.[26,152] Polymeric binders are thus necessary to be incorporated to provide mechanical flexibility/durability and good adhesion to current collectors. Unfortunately, the polymeric binders would also disturb direct contacts between SEs and active materials, thus impeding facile ionic transport network in the composite electrodes.

In summary, the below-par performances of ASLBs are attributed to the afore-discussed incompleteness in ionic contacts and percolation networks in the composite electrodes. To address this issue, excessive amounts of SEs are often used in the composite electrode, lowering the energy density of ASLBs. In the following section, conventional fabrication protocols for sheet-type electrodes are described. Subsequently, applications of solution processes for electrode fabrication are discussed.

5.2. Fabrication of Sheet-Type Electrodes

Figure 8a shows a schematic illustration of the typical fabrication process for sheet-type ASLB electrodes and large-format ASLBs. After the electrode layers are coated on the current collectors, the SE layers can be coated directly onto the as-formed electrodes. The major difference in ASLB electrodes is the inclusion of SE powders during the fabrication of electrodes,[180–182] compared to the injection of liquid electrolytes into the electrode-separator assemblies in the conventional LIBs. Further, the use of Cu current collectors for anodes may be hampered by the chemical reactivity with sulfide materials.[182,183] More importantly, the attempts for the slurry-based fabrication of ASLB electrodes revealed several complications that were not posed for the fabrication of conventional LIB electrodes. First, the use of commonly used polar solvents for LIB electrodes, such as *N*-methyl-2-pyrrolione (NMP) and water, is not allowed due to their severe reaction with sulfide SEs.[72,179] Instead, suitable combinations of nonpolar or less polar solvents (e.g., toluene, xylene) and polymeric binders (e.g., nitrile–butadiene

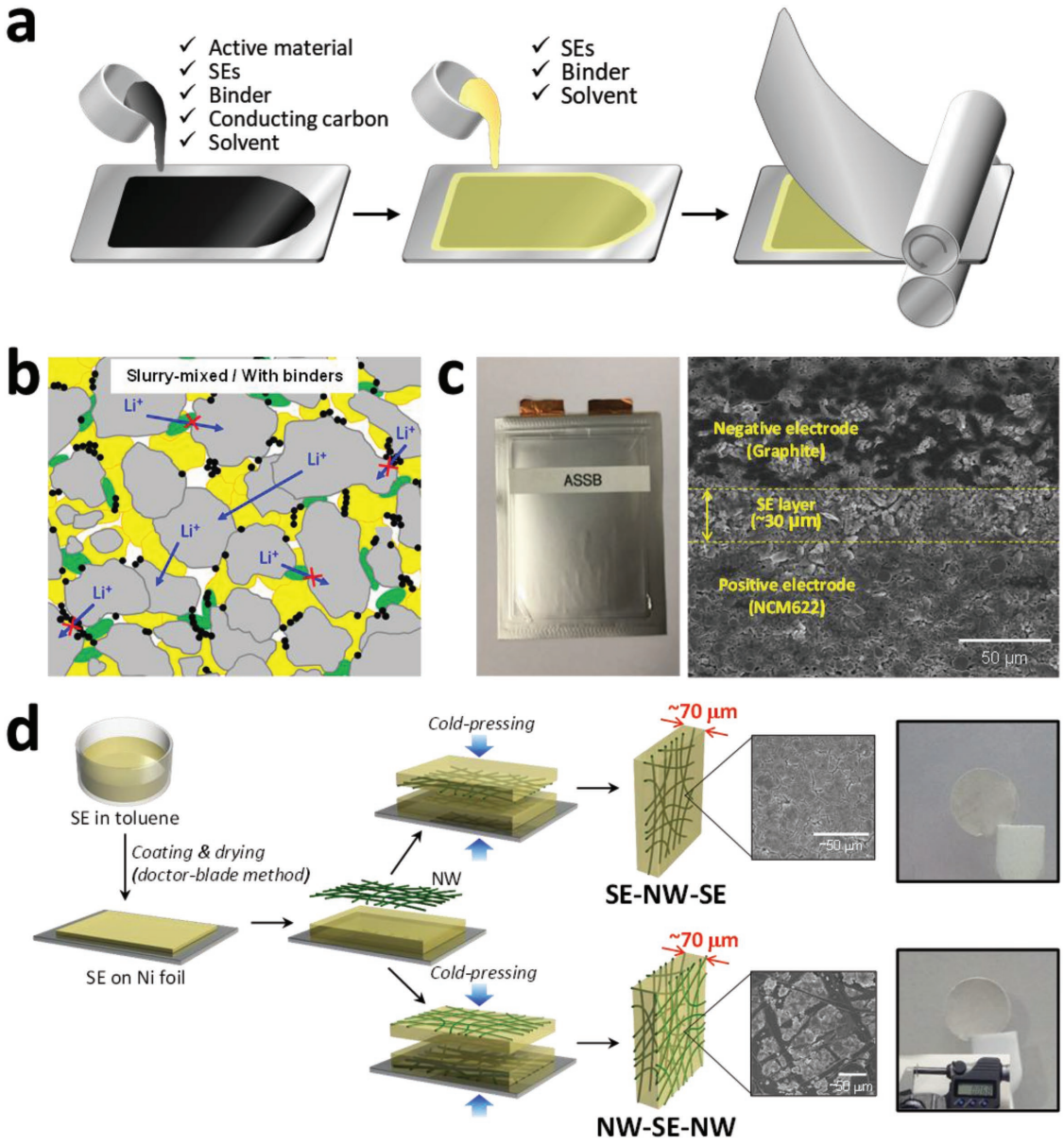

Figure 8. Fabrication of sheet-type electrode and SE films for ASLBs. a) Schematic diagram illustrating slurry-based fabrication of sheet-type electrodes and SE layers for ASLBs. b) Schematic diagram of microstructure of slurry-mixed electrodes for ASLBs. c) Photograph of a pouch-type $LiNi_{0.6}Co_{0.2}Mn_{0.2}O_2$/graphite ASLB and its cross-sectional FESEM image. Reproduced with permission.[182] Copyright 2017, Elsevier. d) Schematic diagram showing the fabrication of bendable nonwoven (NW)-SE films. Reproduced with permission.[26] Copyright 2015, the American Chemical Society.

rubber (NBR), styrene–butadiene rubber, and silicone rubber) should be developed.[180,182,184] This can be challenging because many aspects must be satisfied simultaneously; e.g., volatility and toxicity of the solvents, viscosity of the slurry, and the adhesion property of the resulting electrode layers onto the current collectors. Second, the slurry-mixing process for ASLB electrodes is much more complicated than that for LIB electrodes with respect to the number of components. For ASLBs, a balance in ionic and electronic contacts/connectivity should be adjusted in the mixing of three components (active materials, SE, and carbon additives) while only the electronic contacts/connectivity is crucial for LIB electrodes (active materials and carbon additives).[152] Specifically, the composite structure architecture and the resulting Li^+ and electronic transport percolation network on the performance should be much more complex for ASLB electrodes than for LIB electrodes. While liquid electrolytes wet carbon additives and soak the polymeric binders easily, SEs may not fully access all active materials unless complete contact and ionic/electronic transport network are formed (Figure 8b). The area for ionic conduction at the surface of active materials are in competition with those for electronic conduction (carbon additives) and mechanical adhesion (polymeric binders). In short, the appropriate combination of each components and electrode engineering to ensure

favorable charge-carrier transports are imperative for sheet-type ASLB electrodes.

To date, only a few results on practically relevant prototype ASLBs using sheet-type electrodes have been reported.[180–182] Recently, Jung and co-workers demonstrated a cell-based energy density of 184 W h kg^{-1} for the pouch-type 80 × 60 mm^2 $LiNi_{0.6}Co_{0.2}Mn_{0.2}O_2$/graphite ASLBs (Figure 8c).[182] Further, their robustness against high-temperature (111 °C) exposure and scissor-cutting abusement was demonstrated for the first time. However, the performances of sheet-type ASLBs are limited by poor ionic contact when SE fraction is lowered and thicker electrode is used, which calls for the need to improve the conductivity of SEs and to enhance the ionic contacts.

Recently, an unconventional one-step fabrication protocol for sheet-type ASLB electrodes was developed.[185] Instead of using SE powders, SE precursors (Li_2S and P_2S_5) were directly employed to form the electrode slurry based on NBR and THF.

The protocol of direct SE-layer coatings on preformed electrodes lessens engineering efforts for separators, but still suffers from several technical issues: i) difficulty in precise thickness control of SE layers on large-area electrodes; ii) poor mechanical flexibility of SE layers; and iii) interlayer-mixing between preformed electrode layers and SE layers during the coating process (Figure 8a).[180,182] In this regard, similar to the case for conventional LIBs, assembling separately prepared electrodes and SE films may be a solution. The fabrication of the first bendable sulfide SE films with thicknesses of ≤70 µm was achieved by impregnating SE powders (Li_3PS_4 or LGPS) into porous polymeric nonwoven (NW) scaffolds (Figure 8d).[26] Further, the proof-of-concept of free-standing sheet-type $LiCoO_2$/$Li_4Ti_5O_{12}$ ASLBs enabled by the use of bendable SE-NW films and Ni-coated NW current collectors was successfully demonstrated. Moreover, the bipolar cell, which doubled the operating voltages was obtained by stacking two monocells.

5.3. Applications of Solution-Processable Li-Ion SEs for Electrodes

As discussed in the previous sections, complicated issues on ionic contacts between active materials and SEs are imperative for the performance of ASLBs. An important proof-of-concept of sulfide SE ($Li_2S \cdot P_2S_5$) coatings onto active materials ($LiCoO_2$) was shown by using the pulsed-laser deposition technique.[186,187] The electrode using $Li_2S \cdot P_2S_5$-coated $LiCoO_2$ powders could be cycled even with the small amount of coated SEs (1–10 wt%). In this context, the homogenous SE solutions offer a promising scalable protocol for solidifying SEs on the surface of active materials (**Figure 9**a).[21,72,81,153] For this purpose,

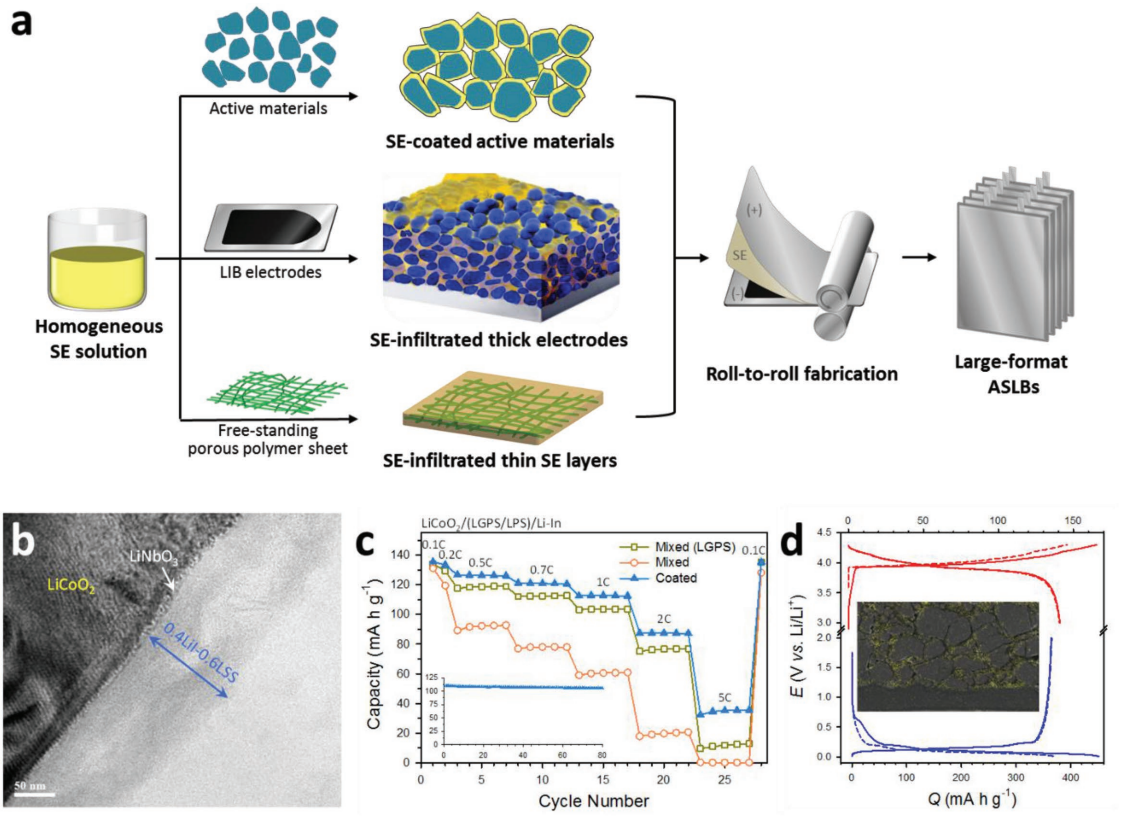

Figure 9. Applications of solution-processable SEs for ASLB electrodes. a) Schematic diagram illustrating fabrication of sheet-type electrodes and ASLBs applying solution process of SEs; coating and infiltration with SEs. b) Cross-sectional HRTEM image of 0.4LiI·0.6Li_4SnS_4-coated $LiCoO_2$ particle. c) Rate capabilities for $LiCoO_2$/Li–In all-solid-state cells using the conventional mixed electrodes and 0.4LiI·0.6Li_4SnS_4-coated electrode. Reproduced with permission.[21] Copyright 2016, Wiley-VCH. d) First two-cycle charge–discharge voltage profiles for $LiCoO_2$/Li–In and graphite/Li–In all-solid-state cells using the Li_6PS_5Cl-infiltrated LIB electrodes at 0.1C and cross-sectional FESEM image of the Li_6PS_5Cl-infiltrated $LiCoO_2$ electrode. Reproduced with permission.[152] Copyright 2017, the American Chemical Society.

multiple requirements must be simultaneously satisfied. First, the high conductivity of solidified electrolytes is required. To avoid side reactions, unfortunately most combinations of phosphorus-containing SEs and protic solvents are ruled out. Second, solvents with cost-effectiveness, no toxicity, and low boiling point are desired. Lastly, the SE solutions should be chemically inert when in contact with the active materials.

Among the listed SE solutions in Section 4.2, only a few can fulfill the aforementioned multiple requirements. Two promising candidates are $LiI{\cdot}Li_4SnS_4$-MeOH or aqueous solutions and Li_6PS_5X-EtOH solutions (X = Cl, Br).[21,152,153,165] The EtOH-solution-processed Li_6PS_5X showed maximum ionic conductivity of (1–2) × 10^{-4} S cm^{-1} at 25 °C.[152,165] Good compatibility of the Li_6PS_5Cl-EtOH solution with $LiCoO_2$ as well as graphite was demonstrated.[152] In addition, higher ionic conductivity was achieved for $0.4LiI{\cdot}0.6Li_4SnS_4$ glass (4.1 × 10^{-4} S cm^{-1} at 30 °C).[21] A disadvantage for $0.4LiI{\cdot}0.6Li_4SnS_4$ is its poor anodic stability under 1 V (vs Li/Li^+), which prohibits the application to graphite electrodes. However, the excellent dry-air stability for $0.4LiI{\cdot}0.6Li_4SnS_4$ is a great strength compared to the phosphorus-containing counterparts such as Li_6PS_5X.

The high-resolution TEM (HRTEM) image (Figure 9b) shows the solution-processed hundreds-of-nanometer-thick uniform coatings of $0.4LiI{\cdot}0.6Li_4SnS_4$ on $LiCoO_2$ particle demonstrated with intimate contacts.[21] Surprisingly, the electrode prepared using the $0.4LiI{\cdot}0.6Li_4SnS_4$-coated $LiCoO_2$ outperformed the electrodes prepared by manual mixing with $0.4LiI{\cdot}0.6Li_4SnS_4$ and even with the state-of-the-art SE LGPS (Figure 9c). Considering more than one order of magnitude higher conductivity of LGPS (6.0 × 10^{-3} S cm^{-1}) than that of $0.4LiI{\cdot}0.6Li_4SnS_4$ (4.1 × 10^{-4} S cm^{-1}), this result made an unprecedented emphasis on the critical importance of ionic contacts and percolations in ASLB electrodes. While the benefits of SE-coated active materials have been demonstrated for the lab-scale pelletized electrodes without using polymeric binders and carbon additives, more significant impact by SE-coatings is expected for the application of sheet-type electrodes where the disruption in ionic contacts and percolation networks would become more severe.

Recently, Jung and co-workers have expanded the application of solution-processable SEs to scalable fabrications of sheet-type electrode inspired by the liquid-electrolyte injection in the manufacturing process for LIBs (Figure 9a).[152] In their approach, the homogeneous SE solutions (Li_6PS_5Cl–EtOH or $LiI{\cdot}Li_4SnS_4$–MeOH) were infiltrated into conventional electrodes for LIBs, which consisted of active materials, carbon, and polyvinylidene fluoride. The SE-infiltrated electrodes for $LiCoO_2$ and graphite were demonstrated to show high capacities of 141 and 364 mA h g^{-1} at 0.1 C with reasonable electrode conditions in terms of the practical application (Figure 9d), which was attributed to favorable ionic contacts/networks; mass loadings of 10 (mg of $LiCoO_2$) cm^{-2} and 6 (mg of graphite) cm^{-2}, low SE weight fractions of 11 wt% for $LiCoO_2$ electrodes and 21 wt% for graphite electrodes. It was highlighted that the commercially available LIB electrodes could be employed for ASLBs without any modification. Further, it will be possible to fabricate bendable SE separating films by infiltrating porous membranes with the SE solutions (Figure 9a).

Overall, all the afore-described applications using homogeneous SE solutions can be combined in the range of active materials, electrodes, and SE layers, to pursue scalable roll-to-roll fabrications of ASLBs (Figure 9a). Although the feasibility of several major concepts has been demonstrated, only a few SEs are known to be solution-processable. Moreover, their ionic conductivities are below par (≈10^{-4} S cm^{-1}). Thus, the search of new solution-processable SEs is required.

6. Na-Ion SEs and ASNBs

Combining renewable energy resources, such as solar and wind power, which suffer from their inherent discontinuity, with large-scale energy storage systems enables reliable power supply.[13,188] Since the cost effectiveness of energy storage system is utmost requirement for this application, Na-ion batteries exploiting abundant Na resource and excluding the use of Cu current collectors are considered as a highly competitive alternative to LIBs.[41] Furthermore, replacing liquid electrolytes with nonflammable inorganic Na^+ SEs can improve safety. Thus, ASNBs are highly pursued for the large-scale energy storage applications.[81,82,189,190]

Similar to the sulfide Li-ion SEs, the development of sulfide Na-ion SEs was initiated from Na_3PS_4 (**Figure 10**a). While LISICON-type Na_3PO_4 shows poor ionic conductivity (≈10^{-8} S cm^{-1} at 100 °C),[191] the replacement of O^{2-} with S^{2-} leads to tetragonal Na_3PS_4 (t-Na_3PS_4) with a moderate ionic conductivity (≈10^{-6}–10^{-5} S cm^{-1} at 25 °C).[18,143,192] By employing mechanochemical methods with the heat-treatment temperature lowered to 270 °C, cubic Na_3PS_4 (c-Na_3PS_4) was obtained, which resulted in Na^+ superionic conductivity (4.6 × 10^{-4} S cm^{-1} at 25 °C).[18,193] The Na^+ conductivity has been enhanced by various iso- or aliovalent substitutions (Figure 10a). The partial aliovalent substitution of P^{5+} with Si^{4+} and Sn^{4+}, rendering Na^+ interstitials, gave highly ionic conductive $94Na_3PS_4{\cdot}6Na_4SiS_4$ (7.4 × 10^{-4} S cm^{-1} at 25 °C)[193,194] and $Na_{3.1}Sn_{0.1}P_{0.9}S_4$ (2.5 × 10^{-4} S cm^{-1} at 25 °C), respectively.[195] Alternatively, introducing Na^+ vacancies by partial substitution of S^{2-} with Cl^- resulted in a high conductivity for $Na_{3-x}PS_{4-x}Cl_x$ (x = 0.625, 1.14 × 10^{-3} S cm^{-1} at 25 °C).[196] The LGPS-type Na analogue $Na_{10}SnP_2S_{12}$ (4 × 10^{-4} S cm^{-1} at 25 °C) was also suggested,[197] and a new Na-ion SE $Na_{11}Sn_2PS_{12}$ (3.7 × 10^{-3} S cm^{-1} at 25 °C for annealed pellet) was recently reported.[198,199] The isovalent substitution of P^{5+} with As^{5+} led to a remarkable improvement in Na^+ conductivity and atmospheric chemical stability for $Na_3P_{0.62}As_{0.38}S_4$ (1.46 × 10^{-3} S cm^{-1} at 25 °C).[139,200] However, the use of toxic element arsenic would not allow its practical application. Alternatively, the isovalent substitutions with large ions Se^{2-} (198 vs 184 pm for S^{2-}) and Sb^{5+} (60 vs 38 pm for P^{5+}) enabled Na_3PSe_4 (1.16 × 10^{-3} S cm^{-1} at 25 °C)[201] and Na_3SbS_4 ((1–3) × 10^{-3} S cm^{-1} at 25 °C) with high conductivities.[81,202] Very recently, the drastic transition from insulating Na_4SnS_4 to highly conducting $Na_{4-x}Sn_{1-x}Sb_xS_4$ ($0.02 \le x \le 0.33$) by aliovalent substitution was reported.[82] This unprecedented crystal structure showed a maximum conductivity of 5.0 × 10^{-4} S cm^{-1} at 30 °C. It should be emphasized that phosphorus-free compounds of Na_3SbS_4 and Sb-substituted Na_4SnS_4 do not suffer from the evolution of toxic H_2S gases in contact with water, in sharp contrast to conventional Na_3PS_4 SEs.[81,82]

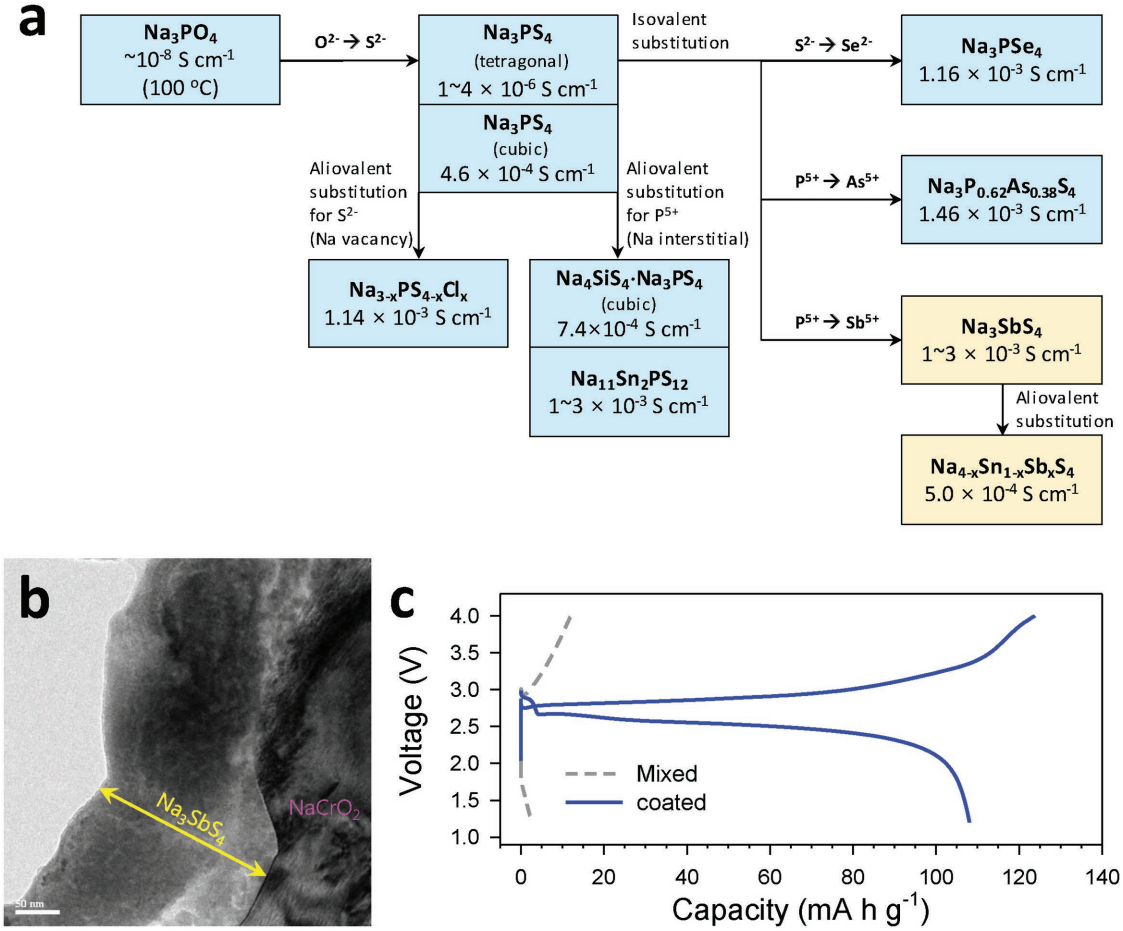

Figure 10. Progresses in Na^+ superionic conductors and ASNBs. a) Design strategy for Na^+ superionic conductors. Na-ion SEs which are solution-processable and show no H_2S evolution in contact with water are emphasized in the box in yellow. b) Cross-sectional HRTEM image of $NaCrO_2$ coated with Na_3SbS_4 by solution process using MeOH. c) The first-cycle charge–discharge voltage profiles for $NaCrO_2$/Na–Sn ASNBs at 50 μA cm^{-2}, using the conventional mixed electrode and the Na_3SbS_4-coated electrode. Reproduced with permission.[81] Copyright 2016, Wiley-VCH.

First principles calculations have been performed to understand the diffusion mechanisms in Na-based sulfide SEs as well as to predict new compositions and structures as novel Na-ion SEs. AIMD simulations studies revealed that Na^+ diffusion in both t-Na_3PS_4 and c-Na_3PS_4 are mediated by vacancy or interstitial mobile carriers. In AIMD simulations, negligible diffusion is found in the perfect stoichiometric composition with no carrier[203,204] and high Na^+ conductivity is activated once vacancies or interstitials are introduced into the structure through the aliovalent doping for P cations or S anions (**Figure 11**a).[143,196,203,204] First principles computation by Ong and co-workers[203] found 6.25% doping of Si^{4+} for P^{5+} in c-Na_3PS_4 with interstitials achieving a Na^+ conductivity of >10^{-3} S cm^{-1} at RT (Figure 11a,b), which agreed with previous experimental results.[193,194] First principles computation also predicted halogen doping for S in t-Na_3PS_4 with more Na^+ vacancies as an effective strategy to increase Na^+ conductivity.[194,196] As a result, novel Cl-doped t-Na_3PS_4 SE, t-$Na_{3-x}PS_{4-x}Cl_x$, with a Na^+ conductivity exceeding 10^{-3} S cm^{-1} at RT was computationally predicted and experimentally synthesized and confirmed.[196] In addition, this newly predicted SE has been applied in RT all-solid-state rechargeable Na-ion battery with sodium metal anode.[196]

The Na^+ diffusion mechanisms in these SEs were found to be consistent with the Li^+ diffusion mechanism in Li superionic conductors (Section 2.3). AIMD simulations revealed the strong correlation in Na^+ migration in Na_3PS_4,[203] which was consistent with the generally observed concerted migration mechanisms in fast Li-ion conductors.[87] In addition, the general design principles based on the bcc-type anion structural framework for fast alkali-ion conductors were also demonstrated to be applicable to Na-ion conductors (Figure 11c). Based on this design principle, computational studies by Ceder and co-workers predicted new Na sulfide SEs, such as $Na_{10}MS_2P_{12}$ (M = Ge, Sn, Si)[197,205] and $Na_7P_3S_{11}$[206] (Figure 11c), which exhibit decent phase stability and high Na^+ ionic conductivity of 1–10 × 10^{-3} and 1 × 10^{-2} S cm^{-1}, respectively, at RT. These computation studies indicate significant potentials in further discovery of novel fast Na^+ conducting SEs based on the rational design strategies and predictive first principles computations.

First principles calculations were also performed to investigate electrochemical stability and interface compatibilities of sodium sulfide SEs.[105,196] The thermodynamic intrinsic electrochemical window of Na_3PS_4 was calculated to be 1.55 to 2.25 V (vs Na/Na^+) (Figure 11d). The sodiation reduction products of

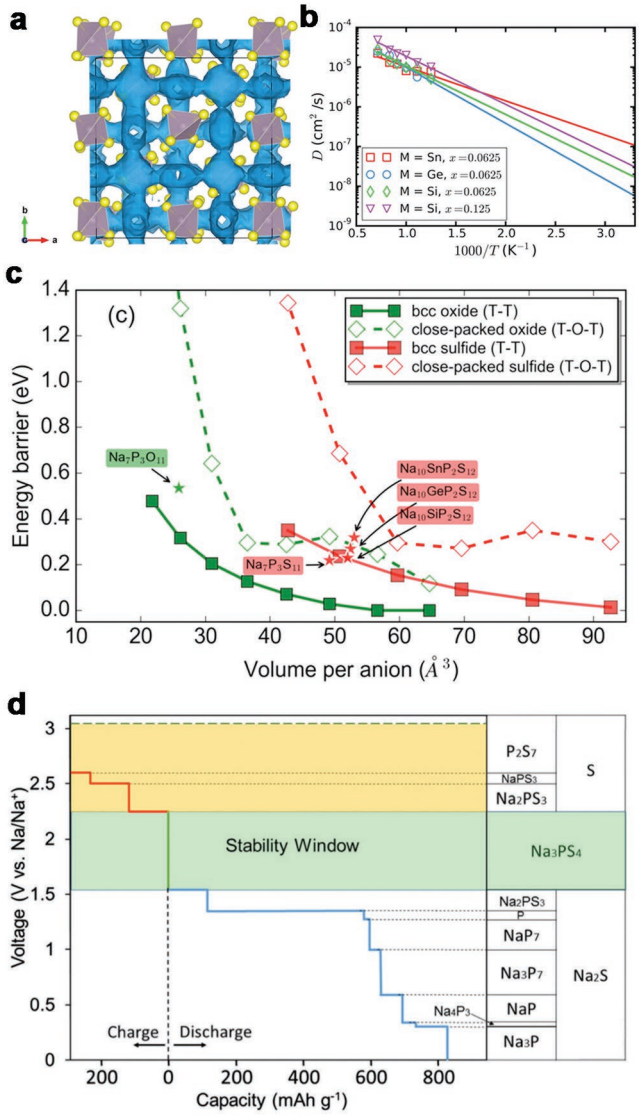

Figure 11. a) Na ion probability density (blue) for $Na_{3+x}Si_xP_{1-x}S_4$ (x = 0.0625) from AIMD simulations at 800 K. b) Arrhenius plots of $Na_{3+x}M_xP_{1-x}S_4$ (M = Si, Ge, Sn) from AIMD simulations. Reproduced with permission.[203] Copyright 2015, the American Chemical Society. c) Calculated migration energy barriers for Na^+ diffusion in bcc and fcc anion (O^{2-} and S^{2-}) lattices as a function of volume per anion. Reproduced with permission.[206] Copyright 2017, the American Chemical Society. d) Voltage profile of Na_3PS_4. Reproduced with permission.[105] Copyright 2017, the Royal Society of Chemistry.

Na_3PS_4 at Na metal anode are Na_2S and Na_3P. Na_3P has a small band gap and is electronically conducting, leading to the formation of MIEC interphase layers, in agreement with experimental observation of in situ XPS by Janek and co-workers.[103] At voltages above 2.25 V, the oxidation reaction becomes favorable, and the oxidation products such as Na_2PS_3, $NaPS_3$, and S, may form at the interface. Doped Na_3PS_4 can form different interfacial products at the Na anode from first principles calculations. Si- and Sn-doped Na_3PS_4 may form electronically conducting Na–Si and Na–Sn alloy compounds, respectively, at low voltages.[203] The interphase including NaCl may be formed in Cl-doped Na_3PS_4 as shown by first principles computation.[196] The chemical reaction between Na_3PS_4 SE and $NaMO_2$ (M = Cr, Mn, Fe, Co, Ni) cathode materials was also found to be favorable in first principles computation,[105] similar to Li-ion sulfide SEs and oxide cathode interfaces. The interfacial reactions occurred through the anion exchange reaction, e.g., in NPS and $NaCrO_2$ to form Na_3PO_4 and $NaCrS_2$. For other cathodes $NaCoO_2$ and $NaNiO_2$, the interfaces underwent redox reaction of Co and Ni to form Ni sulfides and Co sulfides. Similar to ASLBs, the interface compatibility is also a critical issue to be resolved in ASNBs.

As demonstrated in the case of ASLBs, the formation of intimate ionic contacts in composite electrodes is also imperative for the performance of ASNBs. Interestingly, it was demonstrated that Na_3SbS_4 can be dissolved into water or MeOH without the evolution of H_2S gases, forming homogeneous SE solutions.[81] As described in Section 4, the Na-ion SE solutions could be solidified on the surface of active materials (Figure 10b). The $NaCrO_2$/Na-Sn ASNBs employing the resulting Na_3SbS_4-coated $NaCrO_2$ showed dramatically improved performances at RT, compared with those employing the conventional mixture electrodes (Figure 10c).[81] Recently, another phosphorus-free compound, Sb-doped Na_4SnS_4 ($Na_{4-x}Sn_{1-x}Sb_xS_4$), has also been shown to be solution-processable using water.[82] Moreover, the aqueous-solution synthetic route for Na_3SbS_4 using precursors of Na_2S, Sb_2S_3, and S, which allow the coating of Na_3SbS_4 on FeS_2 for FeS_2/Na-Sn ASNBs, was recently developed.[190]

It is worth mentioning several key issues for the realization of room-temperature ASNBs using sulfide Na-ion SEs. To achieve high working voltages, oxide-based cathode materials that have been investigated in the field of Na-ion batteries[41] should be employed. However, the reactivity between active materials and SEs is still a major challenge,[105] and the development of advanced protective coatings is indispensable. These coatings can also contribute to the suppression of side reactions for active materials in contact with solutions for the solution process of SEs.[72] Second, the inherently poor anodic instability of SEs needs to be addressed to suppress the formation of MIEC interphase layers on negative electrodes, calling for a cell design with multiple SE layers or anode protective coating.

7. Summary and Outlook

Since the early discoveries of sulfide Li^+ superionic conductors such as thio-LISICON and $Li_2S{\cdot}P_2S_5$ glass-ceramics, a number of compounds showing high conductivities have been developed to date. While the majority of discoveries have been achieved through intensive trial-and-error exploration of the multicomponent systems, noticeable advances in the first principles computation technique in recent years have enabled the accelerated search for stronger candidates. Thus, it is highly anticipated that more superior superionic conductor SEs to conventional liquid electrolytes will be identified in the future. Recently, much attention in this field has been expanded to other critical issues for sulfide SEs, such as atmospheric instability and yet-brittle mechanical property, which hamper a realistic design and the production protocols of large-format all-solid-state batteries in terms of practical applications. In this regard, the

research in the future should provide not only highly conductive but also chemically stable sulfide SEs as a high priority. Rational designs in compositions, such as partial substitution of sulfur with oxygen, which may be offset by lowered conductivity, rigorous exploration of phosphorus-free materials such as Sn-based compounds (e.g., $LiI{\cdot}Li_4SnS_4$), and surface modifications can be potential directions. Considering the narrow thermodynamic electrochemical windows for sulfide materials, the engineering for stable interfaces between active materials and SEs is also imperative for high-performance all-solid-state batteries. Developments of advanced materials and design for interfacial architectures may enable the use of high-voltage cathode materials operating at ≥5 V (vs Li/Li^+), high-capacity Li_2S (or S), and the ultimate anode Li metal, opening unprecedented opportunities in the LIB field. The recent advances in the solution-processable SEs are also highly noteworthy as they have provided the proof-of-concept of achieving intimate ionic contacts between active materials and SEs in all-solid-sate batteries for practical applications.

It is noteworthy that electrochemical behaviors for all-solid-state batteries are highly affected by mechanical environments, which are often overlooked. For the conventional LIBs, the volume changes in active materials cause concerns in electrical connectivity while the integrity of the electrodes and cells remains relatively intact. By contrast, for all-solid-state batteries, the effects of the mechanical degradation caused by the repeated volume changes in active materials are profound. Thus, the cell performance for all-solid-state batteries are greatly affected by externally applied pressure. In this regard, studies on the performance of all-solid-state batteries relevant to applied pressure would be important.[175,207,208] The critical problem of internal short circuit caused by the penetrating growth of Li metal through SEs led to the routine use of In or Li–In alloys as the counter electrode and simultaneously as the reference electrode for all-solid-state Li-ion half-cells. However, its reliability has not yet been evaluated. Further, practically relevant all-solid-state full-cells have rarely been investigated. These call for the need to develop an all-solid-state three-electrode cell. Unfortunately, its development is challenging because of the unique fabrication protocol for all-solid-state batteries based on cold-pressing at high pressure of hundreds of MPa. Recently, Jung and co-workers have developed a reliable all-solid-state three-electrode cell that enables the diagnosis of failure modes for all-solid-state batteries.[209] In-depth analysis at the interfaces of active materials and SEs using in situ methods (e.g., in situ SEM,[131] XPS,[110] XRD,[175] TEM,[87] Raman,[210] and electron holography[211]) is also required for the understanding of complex interfacial chemistries.

Inspired by the progresses in sulfide Li-ion SE materials, several Na^+ superionic conductors have been discovered to date. The sulfide Na-ion SE materials also have issues that are in common with the Li-ion counterparts (e.g., air-stability, electrochemical stability, and solution processability). Specifically, the poor anodic and cathodic interface stability of sulfide Na-ion SEs, stemming from the nonpassivating decomposition reactions, is a critical issue for the realization of high-energy ASNBs. Considering the extensive progresses in ASLBs and Na-ion batteries, further efforts to develop ASNBs are desired. Very recently, high Mg^{2+} conductivity has been achieved for the selenide compound $MgSc_2Se_4$ (≈10^{-5}–10^{-4} S cm^{-1} at 25 °C), suggesting the potential for all-solid-state Mg batteries.[212] Following the recent progress in K-ion batteries,[40,42,213] the exploration for K-ion SEs and all-solid-sate K batteries would be of interest as well.

Acknowledgements

K.H.P. and Q.B. contributed equally to this work. K.H.P., D.H.K., D.Y.O., and Y.S.J. were supported by the Technology Development Program to Solve Climate Changes and by Basic Science Research Program through the National Research Foundation of Korea (NRF) funded by the Ministry of Science, ICT & Future Planning (Nos. NRF-2017M1A2A2044501 and NRF-2018R1A2B6004996), and by the Materials and Components Technology Development Program of MOTIE/KEIT (10077709). Q.B., Y.Z., and Y.M. were supported by the U.S. Department of Energy, Office of Energy Efficiency and Renewable Energy, under Award Nos. DE-EE0006860 and DE-EE0007807.

Conflict of Interest

The authors declare no conflict of interest.

Keywords

first principles calculations, solid electrolytes, solid-state batteries, sulfides, superionic conductors

Received: January 5, 2018
Revised: February 24, 2018
Published online:

[1] M. S. Whittingham, *Science* **1976**, *192*, 1126.
[2] M. Mohri, N. Yanagisawa, Y. Tajima, H. Tanaka, T. Mitate, S. Nakajima, M. Yoshida, Y. Yoshimoto, T. Suzuki, H. Wada, *J. Power Sources* **1989**, *26*, 545.
[3] T. Nagaura, K. Tozawa, *Prog. Batteries Solar Cells* **1990**, *9*, 209.
[4] R. Fong, U. von Sacken, J. R. Dahn, *J. Electrochem. Soc.* **1990**, *137*, 2009.
[5] F. Orsini, A. du Pasquier, B. Beaudouin, J. M. Tarascon, M. Trentin, N. Langenhuizen, E. de Beer, P. Notten, *J. Power Sources* **1999**, *81–82*, 918.
[6] D. Aurbach, E. Zinigrad, Y. Cohen, H. Teller, *Solid State Ionics* **2002**, *148*, 405.
[7] X.-B. Cheng, R. Zhang, C.-Z. Zhao, Q. Zhang, *Chem. Rev.* **2017**, *117*, 10403.
[8] K. Xu, *Chem. Rev.* **2004**, *104*, 4303.
[9] Y. S. Jung, P. Lu, A. S. Cavanagh, C. Ban, G.-H. Kim, S.-H. Lee, S. M. George, S. J. Harris, A. C. Dillon, *Adv. Energy Mater.* **2013**, *3*, 213.
[10] P. Arora, Z. Zhang, *Chem. Rev.* **2004**, *104*, 4419.
[11] H. Wu, D. Zhuo, D. Kong, Y. Cui, *Nat. Commun.* **2014**, *5*, 5193.
[12] Y. S. Jung, A. S. Cavanagh, L. Gedvilas, N. E. Widjonarko, I. D. Scott, S.-H. Lee, G.-H. Kim, S. M. George, A. C. Dillon, *Adv. Energy Mater.* **2012**, *2*, 1022.
[13] J. B. Goodenough, Y. Kim, *Chem. Mater.* **2010**, *22*, 587.
[14] M. M. Thackeray, C. Wolverton, E. D. Isaacs, *Energy Environ. Sci.* **2012**, *5*, 7854.
[15] A. Manthiram, X. Yu, S. Wang, *Nat. Rev. Mater.* **2017**, *2*, 16103.

[16] N. Kamaya, K. Homma, Y. Yamakawa, M. Hirayama, R. Kanno, M. Yonemura, T. Kamiyama, Y. Kato, S. Hama, K. Kawamoto, A. Mitsui, *Nat. Mater.* **2011**, *10*, 682.
[17] A. Aboulaich, R. Bouchet, G. Delaizir, V. Seznec, L. Tortet, M. Morcrette, P. Rozier, J.-M. Tarascon, V. Viallet, M. Dollé, *Adv. Energy Mater.* **2011**, *1*, 179.
[18] A. Hayashi, K. Noi, A. Sakuda, M. Tatsumisago, *Nat. Commun.* **2012**, *3*, 856.
[19] Y. Wang, W. D. Richards, S. P. Ong, L. J. Miara, J. C. Kim, Y. Mo, G. Ceder, *Nat. Mater.* **2015**, *14*, 1026.
[20] Y. S. Jung, D. Y. Oh, Y. J. Nam, K. H. Park, *Israel J. Chem.* **2015**, *55*, 472.
[21] K. H. Park, D. Y. Oh, Y. E. Choi, Y. J. Nam, L. Han, J.-Y. Kim, H. Xin, F. Lin, S. M. Oh, Y. S. Jung, *Adv. Mater.* **2016**, *28*, 1874.
[22] Y. Kato, S. Hori, T. Saito, K. Suzuki, M. Hirayama, A. Mitsui, M. Yonemura, H. Iba, R. Kanno, *Nat. Energy* **2016**, *1*, 16030.
[23] J. Janek, W. G. Zeier, *Nat. Energy* **2016**, *1*, 16141.
[24] J. C. Bachman, S. Muy, A. Grimaud, H.-H. Chang, N. Pour, S. F. Lux, O. Paschos, F. Maglia, S. Lupart, P. Lamp, L. Giordano, Y. Shao-Horn, *Chem. Rev.* **2016**, *116*, 140.
[25] K. Kerman, A. Luntz, V. Viswanathan, Y.-M. Chiang, Z. Chen, *J. Electrochem. Soc.* **2017**, *164*, A1731.
[26] Y. J. Nam, S. J. Jo, D. Y. Oh, J. M. Im, S. Y. Kim, J. H. Song, Y. G. Lee, S. Y. Lee, Y. S. Jung, *Nano Lett.* **2015**, *15*, 3317.
[27] P. G. Bruce, *Solid State Electrochemistry*, Cambridge University Press, Cambridge **1995**.
[28] M. Doyle, T. F. Fuller, J. Newman, *Electrochim. Acta* **1994**, *39*, 2073.
[29] B. Wang, J. B. Bates, F. X. Hart, B. C. Sales, R. A. Zuhr, J. D. Robertson, *J. Electrochem. Soc.* **1996**, *143*, 3203.
[30] J. B. Bates, N. J. Dudney, B. Neudecker, A. Ueda, C. D. Evans, *Solid State Ionics* **2000**, *135*, 33.
[31] D. Benrabah, J. Y. Sanchez, M. Armand, *Electrochim. Acta* **1992**, *37*, 1737.
[32] W. H. Meyer, *Adv. Mater.* **1998**, *10*, 439.
[33] L. Long, S. Wang, M. Xiao, Y. Meng, *J. Mater. Chem. A* **2016**, *4*, 10038.
[34] M. Kotobuki, H. Munakata, K. Kanamura, Y. Sato, T. Yoshida, *J. Electrochem. Soc.* **2010**, *157*, A1076.
[35] K. H. Kim, Y. Iriyama, K. Yamamoto, S. Kumazaki, T. Asaka, K. Tanabe, C. A. J. Fisher, T. Hirayama, R. Murugan, Z. Ogumi, *J. Power Sources* **2011**, *196*, 764.
[36] A. Sakuda, A. Hayashi, M. Tatsumisago, *Sci. Rep.* **2013**, *3*, 2261.
[37] Y. Seino, T. Ota, K. Takada, A. Hayashi, M. Tatsumisago, *Energy Environ. Sci.* **2014**, *7*, 627.
[38] A. Jain, S. P. Ong, G. Hautier, W. Chen, W. D. Richards, S. Dacek, S. Cholia, D. Gunter, D. Skinner, G. Ceder, K. A. Persson, *APL Mater.* **2013**, *1*, 011002.
[39] A. D. Sendek, Q. Yang, E. D. Cubuk, K.-A. N. Duerloo, Y. Cui, E. J. Reed, *Energy Environ. Sci.* **2017**, *10*, 306.
[40] H. Kim, J. C. Kim, S.-H. Bo, T. Shi, D.-H. Kwon, G. Ceder, *Adv. Energy Mater.* **2017**, *7*, 1700098.
[41] N. Yabuuchi, K. Kubota, M. Dahbi, S. Komaba, *Chem. Rev.* **2014**, *114*, 11636.
[42] H. Kim, D.-H. Seo, J. C. Kim, S.-H. Bo, L. Liu, T. Shi, G. Ceder, *Adv. Mater.* **2017**, *29*, 1702480.
[43] K.-K. Lee, K. Park, H. Lee, Y. Noh, D. Kossowska, K. Kwak, M. Cho, *Nat. Commun.* **2017**, *8*, 14658.
[44] Y. Y. Ren, K. Chen, R. J. Chen, T. Liu, Y. B. Zhang, C. W. Nan, *J. Am. Ceram. Soc.* **2015**, *98*, 3603.
[45] S. Adams, J. Swenson, *Phys. Chem. Chem. Phys.* **2002**, *4*, 3179.
[46] A. Garcia, G. Torres-Trevin˜o, A. R. West, *Solid State Ionics* **1990**, *40-41*, 13.
[47] R. Kanno, M. Murayama, *J. Electrochem. Soc.* **2001**, *148*, A742.
[48] M. Kraft, S. P. Culver, M. Calderon, F. Boecher, T. Krauskopf, A. Senyshyn, C. Dietrich, A. Zevalkink, J. Janek, W. G. Zeier, *J. Am. Chem. Soc.* **2017**, *139*, 10909.
[49] J. Maier, *Nat. Mater.* **2005**, *4*, 805.
[50] W. Liu, S. W. Lee, D. Lin, F. Shi, S. Wang, A. D. Sendek, Y. Cui, *Nat. Energy* **2017**, *2*, 17035.
[51] C. C. Liang, *J. Electrochem. Soc.* **1973**, *120*, 1289.
[52] H. Tsukasaki, S. Mori, H. Morimoto, A. Hayashi, M. Tatsumisago, *Sci. Rep.* **2017**, *7*, 4142.
[53] C. Dietrich, M. Sadowski, S. Sicolo, D. A. Weber, S. J. Sedlmaier, K. S. Weldert, S. Indris, K. Albe, J. Janek, W. G. Zeier, *Chem. Mater.* **2016**, *28*, 8764.
[54] F. Mizuno, A. Hayashi, K. Tadanaga, M. Tatsumisago, *Adv. Mater.* **2005**, *17*, 918.
[55] F. Mizuno, A. Hayashi, K. Tadanaga, M. Tatsumisago, *Solid State Ionics* **2006**, *177*, 2721.
[56] M. Tachez, J.-P. Malugani, R. Mercier, G. Robert, *Solid State Ionics* **1984**, *14*, 181.
[57] K. Homma, M. Yonemura, T. Kobayashi, M. Nagao, M. Hirayama, R. Kanno, *Solid State Ionics* **2011**, *182*, 53.
[58] B. R. Shin, Y. J. Nam, D. Y. Oh, D. H. Kim, J. W. Kim, Y. S. Jung, *Electrochim. Acta* **2014**, *146*, 395.
[59] M. Ribes, B. Barrau, J. L. Souquet, *J. Non-Cryst. Solids* **1980**, *38–39*, 271.
[60] R. Mercier, J. P. Malugani, B. Fahys, G. Robert, *Solid State Ionics* **1981**, *5*, 663.
[61] H. Wada, M. Menetrier, A. Levasseur, P. Hagenmuller, *Mat. Res. Bull.* **1983**, *18*, 189.
[62] J. H. Kennedy, Z. Zhang, *J. Electrochem. Soc.* **1988**, *135*, 859.
[63] J. H. Kennedy, Z. Zhang, *Solid State Ionics* **1988**, *28*, 726.
[64] Z. M. Zhang, J. H. Kennedy, *Solid State Ionics* **1990**, *38*, 217.
[65] R. Sakamoto, M. Tatsumisago, T. Minami, *J. Phys. Chem. B* **1999**, *103*, 4029.
[66] H.-J. Deiseroth, S.-T. Kong, H. Eckert, J. Vannahme, C. Reiner, T. Zaiss, M. Schlosser, *Angew. Chem., Int. Ed.* **2008**, *47*, 755.
[67] H. Yamane, M. Shibata, Y. Shimane, T. Junke, Y. Seino, S. Adams, K. Minami, A. Hayashi, M. Tatsumisago, *Solid State Ionics* **2007**, *178*, 1163.
[68] C. Dietrich, D. A. Weber, S. J. Sedlmaier, S. Indris, S. P. Culver, D. Walter, J. Janek, W. G. Zeier, *J. Mater. Chem. A* **2017**, *5*, 18111.
[69] Z. D. Hood, C. Kates, M. Kirkham, S. Adhikari, C. Liang, N. A. W. Holzwarth, *Solid State Ionics* **2016**, *284*, 61.
[70] J. F. Brice, *CR Acad Sci. C* **1976**, *283*, 581.
[71] T. Kaib, S. Haddadpour, M. Kapitein, P. Bron, C. Schroeder, H. Eckert, B. Roling, S. Dehnen, *Chem. Mater.* **2012**, *24*, 2211.
[72] Y. E. Choi, K. H. Park, D. H. Kim, D. Y. Oh, H. R. Kwak, Y.-G. Lee, Y. S. Jung, *ChemSusChem* **2017**, *10*, 2605.
[73] J. A. Brant, D. M. Massi, N. A. W. Holzwarth, J. H. MacNeil, A. P. Douvalis, T. Bakas, S. W. Martin, M. D. Gross, J. A. Aitken, *Chem. Mater.* **2015**, *27*, 189.
[74] T. Holzmann, L. M. Schoop, M. N. Ali, I. Moudrakovski, G. Gregori, J. Maier, R. J. Cavad, B. V. Lotsch, *Energy Environ. Sci.* **2016**, *9*, 2578.
[75] P. Bron, S. Johansson, K. Zick, J. Schmedt auf der Günne, S. Dehnen, B. Roling, *J. Am. Chem. Soc.* **2013**, *135*, 15694.
[76] A. Kuhn, O. Gerbig, C. Zhu, F. Falkenberg, J. Maier, B. V. Lotsch, *Phys. Chem. Chem. Phys.* **2014**, *16*, 14669.
[77] G. Sahu, Z. Lin, J. Li, Z. Liu, N. Dudney, C. Liang, *Energy Environ. Sci.* **2014**, *7*, 1053.
[78] E. Rangasamy, Z. Liu, M. Gobet, K. Pilar, G. Sahu, W. Zhou, H. Wu, S. Greenbaum, C. Liang, *J. Am. Chem. Soc.* **2015**, *137*, 1384.
[79] S. J. Sedlmaier, S. Indris, C. Dietrich, M. Yavuz, C. Draeger, F. von Seggern, H. Sommer, J. Janek, *Chem. Mater.* **2017**, *29*, 1830.
[80] H. Muramatsu, A. Hayashi, T. Ohtomo, S. Hama, M. Tatsumisago, *Solid State Ionics* **2011**, *182*, 116.

[81] A. Banerjee, K. H. Park, J. W. Heo, Y. J. Nam, C. K. Moon, S. M. Oh, S.-T. Hong, Y. S. Jung, *Angew. Chem., Int. Ed.* **2016**, *55*, 9634.
[82] J. W. Heo, A. Banerjee, K. H. Park, S.-T. Hong, Y. S. Jung, *Adv. Energy Mater.* **2018**, https://doi.org/10.1002/aenm.201702716.
[83] T. Ohtomo, A. Hayashi, M. Tatsumisago, K. Kawamoto, *J. Non-Cryst. Solids* **2013**, *364*, 57.
[84] T. Ohtomo, A. Hayashi, M. Tatsumisago, K. Kawamoto, *J. Mater. Sci.* **2013**, *48*, 4137.
[85] Y. Mo, S. P. Ong, G. Ceder, *Chem. Mater.* **2012**, *24*, 15.
[86] S. P. Ong, Y. Mo, W. D. Richards, L. Miara, H. S. Lee, G. Ceder, *Energy Environ. Sci.* **2013**, *6*, 148.
[87] X. He, Y. Zhu, Y. Mo, *Nat. Commun.* **2017**, *8*, 15893.
[88] N. D. Lepley, N. A. W. Holzwarth, Y. A. Du, *Phys. Rev. B* **2013**, *88*, 104103.
[89] J. Yang, J. S. Tse, *Comput. Mater. Sci.* **2015**, *107*, 134.
[90] V. Thangadurai, S. Narayanan, D. Pinzaru, *Chem. Soc. Rev.* **2014**, *43*, 4714.
[91] D. A. Weber, A. Senyshyn, K. S. Weldert, S. Wenzel, W. Zhang, R. Kaiser, S. Berendts, J. Janek, W. G. Zeier, *Chem. Mater.* **2016**, *28*, 5905.
[92] X. Liang, L. Wang, Y. Jiang, J. Wang, H. Luo, C. Liu, J. Feng, *Chem. Mater.* **2015**, *27*, 5503.
[93] O. Kwon, M. Hirayama, K. Suzuki, Y. Kato, T. Saito, M. Yonemura, T. Kamiyama, R. Kanno, *J. Mater. Chem. A* **2015**, *3*, 438.
[94] I.-H. Chu, H. Nguyen, S. Hy, Y.-C. Lin, Z. Wang, Z. Xu, Z. Deng, Y. S. Meng, S. P. Ong, *ACS Appl. Mater. Interfaces* **2016**, *8*, 7843.
[95] Z. Deng, Z. Zhu, I.-H. Chu, S. P. Ong, *Chem. Mater.* **2017**, *29*, 281.
[96] N. D. Lepley, N. A. W. Holzwarth, Y. A. Du, *Phy. Rev. B* **2013**, *88*, 104103.
[97] A. Al-Qawasmeh, N. A. W. Holzwarth, *J. Electrochem. Soc.* **2016**, *163*, A2079.
[98] A. Al-Qawasmeh, J. Howard, N. A. W. Holzwarth, *J. Electrochem. Soc.* **2017**, *164*, A6386.
[99] Z. Zhu, I.-H. Chu, S. P. Ong, *Chem. Mater.* **2017**, *29*, 2474.
[100] W. D. Richards, Y. Wang, L. J. Miara, J. C. Kim, G. Ceder, *Energy Environ. Sci.* **2016**, *9*, 3272.
[101] W. D. Richards, L. J. Miara, Y. Wang, J. C. Kim, G. Ceder, *Chem. Mater.* **2016**, *28*, 266.
[102] Y. Zhu, X. He, Y. Mo, *J. Mater. Chem. A* **2016**, *4*, 3253.
[103] S. Wenzel, T. Leichtweiss, D. A. Weber, J. Sann, W. G. Zeier, J. Janek, *ACS Appl. Mater. Interfaces* **2016**, *8*, 28216.
[104] S. Wenzel, T. Leichtweiss, D. Kruger, J. Sann, J. Janek, *Solid State Ionics* **2015**, *278*, 98.
[105] Y. Tian, T. Shi, W. D. Richards, J. Li, J. C. Kim, S.-H. Bo, G. Ceder, *Energy Environ. Sci.* **2017**, *10*, 1150.
[106] A. Sakuda, A. Hayashi, M. Tatsumisago, *Chem. Mater.* **2010**, *22*, 949.
[107] Y. Zhu, X. He, Y. Mo, *ACS Appl. Mater. Interfaces* **2015**, *7*, 23685.
[108] F. Han, Y. Zhu, X. He, Y. Mo, C. Wang, *Adv. Energy Mater.* **2016**, *6*, 1501590.
[109] Y. Zhu, X. He, Y. Mo, *Adv. Sci.* **2017**, *4*, 1600517.
[110] S. Wenzel, S. Randau, T. Leichtweiß, D. A. Weber, J. Sann, W. G. Zeier, J. Janek, *Chem. Mater.* **2016**, *28*, 2400.
[111] J. H. Woo, J. E. Trevey, A. S. Cavanagh, Y. S. Choi, S. C. Kim, S. M. George, K. H. Oh, S.-H. Lee, *J. Electrochem. Soc.* **2012**, *159*, A1120.
[112] J. Auvergniot, A. Cassel, J. B. Ledeuil, V. Viallet, V. Seznec, R. Dedryvere, *Chem. Mater.* **2017**, *29*, 3883.
[113] H. Visbal, Y. Aihara, S. Ito, T. Watanabe, Y. Park, S. Doo, *J. Power Sources* **2016**, *314*, 85.
[114] N. Ohta, K. Takada, I. Sakaguchi, L. Zhang, R. Ma, K. Fukuda, M. Osada, T. Sasaki, *Electrochem. Commun.* **2007**, *9*, 1486.
[115] W. Zhang, D. A. Weber, H. Weigand, T. Arlt, I. Manke, D. Schröder, R. Koerver, T. Leichtweiss, P. Hartmann, W. G. Zeier, J. Janek, *ACS Appl. Mater. Interfaces* **2017**, *9*, 17835.
[116] N. Ohta, K. Takada, L. Zhang, R. Ma, M. Osada, T. Sasaki, *Adv. Mater.* **2006**, *18*, 2226.
[117] X. Xu, K. Takada, K. Fukuda, T. Ohnishi, K. Akatsuka, M. Osada, B. T. Hang, K. Kumagai, T. Sekiguchi, T. Sasaki, *Energy Environ. Sci.* **2011**, *4*, 3509.
[118] J. H. Woo, J. J. Travis, S. M. George, S.-H. Lee, *J. Electrochem. Soc.* **2015**, *162*, A344.
[119] Y. Ito, Y. Sakurai, S. Yubuchi, A. Sakuda, A. Hayashi, M. Tatsumisago, *J. Electrochem. Soc.* **2015**, *162*, A1610.
[120] L. Chen, K. Wang, X. Xie, J. Xie, *J. Power Sources* **2007**, *174*, 538.
[121] H. Ota, Y. Sakata, A. Inoue, S. Yamaguchi, *J. Electrochem. Soc.* **2004**, *151*, A1659.
[122] D. Aurbach, K. Gamolsky, B. Markovsky, Y. Gofer, M. Schmidt, U. Heider, *Electrochim. Acta* **2002**, *47*, 1423.
[123] L. El Ouatani, R. Dedryvère, C. Siret, P. Biensan, D. Gonbeau, *J. Electrochem. Soc.* **2009**, *156*, A468.
[124] D. Y. Wang, N. N. Sinha, J. C. Burns, C. P. Aiken, R. Petibon, J. R. Dahn, *J. Electrochem. Soc.* **2014**, *161*, A467.
[125] L. A. Dominey, V. R. Koch, T. J. Blakley, *Electrochim. Acta* **1992**, *37*, 1551.
[126] J. R. Dahn, U. von Sacken, M. W. Juzkow, H. Al-Janaby, *J. Electrochem. Soc.* **1991**, *138*, 2207.
[127] H. Park, T. Yoon, J. Mun, J. H. Ryu, J. J. Kim, S. M. Oh, *J. Electrochem. Soc.* **2013**, *160*, A1539.
[128] H. Yang, K. Kwon, T. M. Devine, J. W. Evans, *J. Electrochem. Soc.* **2000**, *147*, 4399.
[129] W. Xu, J. Wang, F. Ding, X. Chen, E. Nasybulin, Y. Zhang, J.-G. Zhang, *Energy Environ. Sci.* **2014**, *7*, 513.
[130] C. Monroe, J. Newman, *J. Electrochem. Soc.* **2004**, *151*, A880.
[131] M. Nagao, A. Hayashi, M. Tatsumisago, T. Kanetsuku, T. Tsuda, S. Kuwabata, *Phys. Chem. Chem. Phys.* **2013**, *15*, 18600.
[132] L. Porz, T. Swamy, B. W. Sheldon, D. Rettenwander, T. Frömling, H. L. Thaman, S. Berendts, R. Uecker, W. C. Carter, Y.-M. Chiang, *Adv. Energy Mater.* **2017**, *7*, 1701003.
[133] M. Nagao, A. Hayashi, M. Tatsumisago, *Electrochemistry* **2012**, *80*, 734.
[134] A. Kato, A. Hayashi, M. Tatsumisago, *J. Power Sources* **2016**, *309*, 27.
[135] C.-L. Tsai, V. Roddatis, C. V. Chandran, Q. Ma, S. Uhlenbruck, M. Bram, P. Heitjans, O. Guillon, *ACS Appl. Mater. Interfaces* **2016**, *8*, 10617.
[136] X. Han, Y. Gong, K. K. Fu, X. He, G. T. Hitz, J. Dai, A. Pearse, B. Liu, H. Wang, G. Rubloff, Y. Mo, V. Thangadurai, E. D. Wachsman, L. Hu, *Nat. Mater.* **2017**, *16*, 572.
[137] M. Nagao, A. Hayashi, M. Tatsumisago, T. Ichinose, T. Ozaki, Y. Togawa, S. Mori, *J. Power Sources* **2015**, *274*, 471.
[138] T. Kobayashi, Y. Imade, D. Shishihara, K. Homma, M. Nagao, R. Watanabe, T. Yokoi, A. Yamada, R. Kanno, T. Tatsumi, *J. Power Sources* **2008**, *182*, 621.
[139] K. Suzuki, M. Tateishi, M. Nagao, Y. Imade, T. Yokoi, M. Hirayama, T. Tatsumi, R. Kanno, *J. Electrochem. Soc.* **2017**, *164*, A6178.
[140] B. R. Shin, Y. S. Jung, *J. Electrochem. Soc.* **2014**, *161*, A154.
[141] T. Hakari, M. Nagao, A. Hayashi, M. Tatsumisago, *J. Power Sources* **2015**, *293*, 721.
[142] M. R. Busche, D. A. Weber, Y. Schneider, C. Dietrich, S. Wenzel, T. Leichtweiss, D. Schröder, W. Zhang, H. Weigand, D. Walter, S. J. Sedlmaier, D. Houtarde, L. F. Nazar, J. Janek, *Chem. Mater.* **2016**, *28*, 6152.
[143] F. Han, J. Yue, X. Fan, T. Gao, C. Luo, Z. Ma, L. Suo, C. Wang, *Nano Lett.* **2016**, *16*, 4521.
[144] R.-c. Xu, X.-h. Xia, S.-h. Li, S.-z. Zhang, X.-l. Wang, J.-p. Tu, *J. Mater. Chem. A* **2017**, *5*, 6310.
[145] R.-c. Xu, X.-h. Xia, X.-l. Wang, Y. Xia, J.-p. Tu, *J. Mater. Chem. A* **2017**, *5*, 2829.

[146] Y. Zhang, K. Chen, Y. Shen, Y. Lin, C.-W. Nan, *Solid State Ionics* **2017**, *305*, 1.
[147] X. Yao, N. Huang, F. Han, Q. Zhang, H. Wan, J. P. Mwizerwa, C. Wang, X. Xu, *Adv. Energy Mater.* **2017**, *7*, 1602923.
[148] M. Eom, S. Son, C. Park, S. Noh, W. T. Nichols, D. Shin, *Electrochim. Acta* **2017**, *230*, 279.
[149] C. Yu, S. Ganapathy, E. R. H. v. Eck, H. Wang, S. Basak, Z. Li, M. Wagemaker, *Nat. Commun.* **2017**, *8*, 1086.
[150] Z. Liu, W. Fu, E. A. Payzant, X. Yu, Z. Wu, N. J. Dudney, J. Kiggans, K. Hong, A. J. Rondinone, C. Liang, *J. Am. Chem. Soc.* **2013**, *135*, 975.
[151] N. H. H. Phuc, K. Morikawa, T. Mitsuhiro, H. Muto, A. Matsuda, *Ionics* **2017**, *23*, 2061.
[152] D. H. Kim, D. Y. Oh, K. H. Park, Y. E. Choi, Y. J. Nam, H. A. Lee, S.-M. Lee, Y. S. Jung, *Nano Lett.* **2017**, *17*, 3013.
[153] S. Yubuchi, S. Teragawa, K. Aso, K. Tadanaga, A. Hayashi, M. Tatsumisago, *J. Power Sources* **2015**, *293*, 941.
[154] N. H. H. Phuc, M. Totani, K. Morikawa, H. Muto, A. Matsuda, *Solid State Ionics* **2016**, *288*, 240.
[155] R. C. Xu, X. H. Xia, Z. J. Yao, X. L. Wang, C. D. Gu, J. P. Tu, *Electrochim. Acta* **2016**, *219*, 235.
[156] S. Ito, M. Nakakita, Y. Aihara, T. Uehara, N. Machida, *J. Power Sources* **2014**, *271*, 342.
[157] X. Yao, D. Liu, C. Wang, P. Long, G. Peng, Y.-S. Hu, H. Li, L. Chen, X. Xu, *Nano Lett.* **2016**, *16*, 7148.
[158] M. Calpa, N. C. Rosero-Navarro, A. Miura, K. Tadanaga, *RSC Adv.* **2017**, *7*, 46499.
[159] Y. Wang, D. Lu, M. Bowden, P. Z. El Khoury, K. S. Han, Z. D. Deng, J. Xiao, J.-G. Zhang, J. Liu, *Chem. Mater.* **2018**, *30*, 990.
[160] Y. Wang, Z. Liu, X. Zhu, Y. Tang, F. Huang, *J. Power Sources* **2013**, *224*, 225.
[161] S. Teragawa, K. Aso, K. Tadanaga, A. Hayashi, M. Tatsumisago, *J. Power Sources* **2014**, *248*, 939.
[162] S. Teragawa, K. Aso, K. Tadanaga, A. Hayashi, M. Tatsumisago, *J. Mater. Chem. A* **2014**, *2*, 5095.
[163] F. Wu, J. T. Lee, A. Magasinski, H. Kim, G. Yushin, *Part. Part. Syst. Char.* **2014**, *31*, 639.
[164] F. Wu, A. Magasinski, G. Yushin, *J. Mater. Chem. A* **2014**, *2*, 6064.
[165] S. Yubuchi, A. Hayashi, M. Tatsumisago, *ECS Meet. Abstr.* **2016**, *MA2016-03*, 1051.
[166] A. C. Luntz, J. Voss, K. Reuter, *J. Phys. Chem. Lett.* **2015**, *6*, 4599.
[167] S. Stegmaier, J. Voss, K. Reuter, A. C. Luntz, *Chem. Mater.* **2017**, *29*, 4330.
[168] Y. Kato, S. Shiotani, K. Morita, K. Suzuki, M. Hirayama, R. Kanno, *J. Phys. Chem. Lett.* **2018**, *9*, 607.
[169] D. Y. Oh, Y. E. Choi, D. H. Kim, Y.-G. Lee, B.-S. Kim, J. Park, H. Sohn, Y. S. Jung, *J. Mater. Chem. A* **2016**, *4*, 10329.
[170] P. Poizot, S. Laruelle, S. Grugeon, L. Dupont, J. M. Tarascon, *Nature* **2000**, *407*, 496.
[171] Y.-G. Guo, J.-S. Hu, L.-J. Wan, *Adv. Mater.* **2008**, *20*, 2878.
[172] L. Ji, Z. Lin, M. Alcoutlabi, X. Zhang, *Energy Environ. Sci.* **2011**, *4*, 2682.
[173] W. J. Li, M. Hirayama, K. Suzuki, R. Kanno, *Solid State Ionics* **2016**, *285*, 136.
[174] W. Zhang, T. Leichtweiß, S. P. Culver, R. Koerver, D. Das, D. A. Weber, W. G. Zeier, J. Janek, *ACS Appl. Mater. Interfaces* **2017**, *9*, 35888.
[175] W. Zhang, D. Schroder, T. Arlt, I. Manke, R. Koerver, R. Pinedo, D. A. Weber, J. Sann, W. G. Zeier, J. Janek, *J. Mater. Chem. A* **2017**, *5*, 9929.
[176] J. Shin, J. Yang, C. Sergey, M.-S. Song, Y.-M. Kang, *Adv. Mater.* **2017**, *4*, 1700128.
[177] C. Zhu, R. E. Usiskin, Y. Yu, J. Maier, *Science* **2017**, *358*, eaao2808.
[178] J. E. Trevey, C. R. Stoldt, S.-H. Lee, *J. Electrochem. Soc.* **2011**, *158*, A1282.
[179] D. Y. Oh, Y. J. Nam, K. H. Park, S. H. Jung, S.-J. Cho, Y. K. Kim, Y.-G. Lee, S.-Y. Lee, Y. S. Jung, *Adv. Energy Mater.* **2015**, *5*, 1500865.
[180] S. Ito, S. Fujiki, T. Yamada, Y. Aihara, Y. Park, T. Y. Kim, S. W. Baek, J. M. Lee, S. Doo, N. Machida, *J. Power Sources* **2014**, *248*, 943.
[181] A. Sakuda, K. Kuratani, M. Yamamoto, M. Takahashi, T. Takeuchi, H. Kobayashi, *J. Electrochem. Soc.* **2017**, *164*, A2474.
[182] Y. J. Nam, D. Y. Oh, S. H. Jung, Y. S. Jung, *J. Power Sources* **2018**, *375*, 93.
[183] S. Jacobs, S. Reiber, M. Edwards, *J. Am. Water Work Assoc.* **1998**, *90*, 62.
[184] K. Lee, S. Kim, J. Park, S. H. Park, A. Coskun, D. S. Jung, W. Cho, J. W. Choi, *J. Electrochem. Soc.* **2017**, *164*, A2075.
[185] D. Y. Oh, D. H. Kim, S. H. Jung, J.-G. Han, N.-S. Choi, Y. S. Jung, *J. Mater. Chem. A* **2017**, *5*, 20771.
[186] A. Sakuda, A. Hayashi, T. Ohtomo, S. Hama, M. Tatsumisago, *Electrochem. Solid-State Lett.* **2010**, *13*, A73.
[187] A. Sakuda, A. Hayashi, T. Ohtomo, S. Hama, M. Tatsumisago, *J. Power Sources* **2011**, *196*, 6735.
[188] B. Dunn, H. Kamath, J.-M. Tarascon, *Science* **2011**, *334*, 928.
[189] J.-J. Kim, K. Yoon, I. Park, K. Kang, *Small Methods* **2017**, *1*, 1700219.
[190] T. W. Kim, K. H. Park, Y. E. Choi, J. Y. Lee, Y. S. Jung, *J. Mater. Chem. A* **2017**, *6*, 840.
[191] J.-F. Brice, B. Majidi, H. Kessler, *Mater. Res. Bull.* **1982**, *17*, 143.
[192] M. Jansen, U. Henseler, *J. Solid State Chem.* **1992**, *99*, 110.
[193] A. Hayashi, K. Noi, N. Tanibata, M. Nagao, M. Tatsumisago, *J. Power Sources* **2014**, *258*, 420.
[194] N. Tanibata, K. Noi, A. Hayashi, M. Tatsumisago, *RSC Adv.* **2014**, *4*, 17120.
[195] R. P. Rao, H. Chen, L. L. Wong, S. Adams, *J. Mater. Chem. A* **2017**, *5*, 3377.
[196] I.-H. Chu, C. S. Kompella, H. Nguyen, Z. Zhu, S. Hy, Z. Deng, Y. S. Meng, S. P. Ong, *Sci. Rep.* **2016**, *6*, 33733.
[197] W. D. Richards, T. Tsujimura, L. J. Miara, Y. Wang, J. C. Kim, S. P. Ong, I. Uechi, N. Suzuki, G. Ceder, *Nat. Commun.* **2016**, *7*, 8.
[198] S. Dehnen, M. Duchardt, B. Roling, U. Ruschewitz, S. Adams, *Angew. Chem., Int. Ed.* **2018**, *57*, 1351.
[199] Z. Zhang, E. Ramos, F. Lalere, A. Assoud, K. Kaup, P. Hartman, L. F. Nazar, *Energy Environ. Sci.* **2018**, *11*, 87.
[200] Z. Yu, S.-L. Shang, J.-H. Seo, D. Wang, X. Luo, Q. Huang, S. Chen, J. Lu, X. Li, Z.-K. Liu, D. Wang, *Adv. Mater.* **2017**, *29*, 1605561.
[201] L. Zhang, K. Yang, J. Mi, L. Lu, L. Zhao, L. Wang, Y. Li, H. Zeng, *Adv. Energy Mater.* **2015**, *5*, 1501294.
[202] L. Zhang, D. Zhang, K. Yang, X. Yan, L. Wang, J. Mi, B. Xu, Y. Li, *Adv. Mater.* **2016**, *3*, 1600089.
[203] Z. Zhu, I.-H. Chu, Z. Deng, S. P. Ong, *Chem. Mater.* **2015**, *27*, 8318.
[204] N. J. J. de Klerk, M. Wagemaker, *Chem. Mater.* **2016**, *28*, 3122.
[205] V. S. Kandagal, M. D. Bharadwaj, U. V. Waghmare, *J. Mater. Chem. A* **2015**, *3*, 12992.
[206] Y. Wang, W. D. Richards, S.-H. Bo, L. J. Miara, G. Ceder, *Chem. Mater.* **2017**, *29*, 7475.
[207] D. M. Piper, T. A. Yersak, S.-H. Lee, *J. Electrochem. Soc.* **2013**, *160*, A77.
[208] J. M. Whiteley, J. W. Kim, C. S. Kang, J. S. Cho, K. H. Oh, S.-H. Lee, *J. Electrochem. Soc.* **2015**, *162*, A711.
[209] Y. J. Nam, K. H. Park, W. H. An, Y. S. Jung, submitted.
[210] L. Sang, R. T. Haasch, A. A. Gewirth, R. G. Nuzzo, *Chem. Mater.* **2017**, *29*, 3029.
[211] K. Yamamoto, Y. Iriyama, T. Asaka, T. Hirayama, H. Fujita, C. A. J. Fisher, K. Nonaka, Y. Sugita, Z. Ogumi, *Angew. Chem., Int. Ed.* **2010**, *49*, 4414.
[212] P. Canepa, S.-H. Bo, G. Sai Gautam, B. Key, W. D. Richards, T. Shi, Y. Tian, Y. Wang, J. Li, G. Ceder, *Nat. Commun.* **2017**, *8*, 1759.

[213] H. Kim, J. C. Kim, M. Bianchini, D.-H. Seo, J. Rodriguez-Garcia, G. Ceder, *Adv. Energy Mater.* **2018**, *8*, 1702384.
[214] M. Murayama, N. Sonoyama, A. Yamada, R. Kanno, *Solid State Ionics* **2004**, *170*, 173.
[215] A. Hayashi, S. Hama, T. Minami, M. Tatsumisago, *Electrochem. Commun.* **2003**, *5*, 111.
[216] G. Sahu, E. Rangasamy, J. Li, Y. Chen, K. An, N. Dudney, C. Liang, *J. Mater. Chem. A* **2014**, *2*, 10396.
[217] S. Boulineau, M. Courty, J.-M. Tarascon, V. Viallet, *Solid State Ionics* **2012**, *221*, 1.
[218] A. Kuhn, V. Duppel, B. V. Lotsch, *Energy Environ. Sci.* **2013**, *6*, 3548.
[219] P. Zhou, J. Wang, F. Cheng, F. Li, J. Chen, *Chem. Commun.* **2016**, *52*, 6091.
[220] S. Ujiie, A. Hayashi, M. Tatsumisago, *Solid State Ionics* **2012**, *211*, 42.
[221] S. Hori, K. Suzuki, M. Hirayama, Y. Kato, T. Saito, M. Yonemura, R. Kanno, *Faraday Discuss.* **2014**, *176*, 83.
[222] M. Park, H.-G. Jung, W. D. Jung, S. Y. Cho, B.-N. Yun, Y. S. Lee, S. Choi, J. Ahn, J. Lim, J. Y. Sung, Y.-J. Jang, J.-P. Ahn, J.-H. Lee, H. Kim, *ACS Energy Lett.* **2017**, *2*, 1740.
[223] S. Chida, A. Miura, N. C. Rosero-Navarro, M. Higuchi, N. H. H. Phuc, H. Muto, A. Matsuda, K. Tadanaga, *Ceram. Int.* **2018**, *44*, 742.